IMMUNOLOGY

Mechanisms of antigen-induced reversal of CNS inflammation in experimental demyelinating disease

Jian Li[1,2]†, Lisen Lu[3]†, Kyle Binder[1,4], Jian Xiong[2], Lilin Ye[2], Yan H. Cheng[1,5], Sonia Majri-Morrison[1], Wei Lu[1], Jae W. Lee[1], Zhihong Zhang[3]*, Yu-zhang Wu[2]*, Lixin Zheng[1,5]*, Michael J. Lenardo[1,5]*

Autoimmune central nervous system (CNS) demyelinating diseases are a major public health burden and poorly controlled by current immunosuppressants. More precise immunotherapies with higher efficacy and fewer side effects are sought. We investigated the effectiveness and mechanism of an injectable myelin-based antigenic polyprotein MMPt (myelin oligodendrocyte glycoprotein, myelin basic protein and proteolipid protein, truncated). We find that it suppresses mouse experimental autoimmune encephalomyelitis without major side effects. MMPt induces rapid apoptosis of the encephalitogenic T cells and suppresses inflammation in the affected CNS. Intravital microscopy shows that MMPt is taken up by perivascular F4/80$^+$ cells but not conventional antigen-presenting dendritic cells, B cells, or microglia. MMPt-stimulated F4/80$^+$ cells induce reactive T cell immobilization and apoptosis in situ, resulting in reduced infiltration of inflammatory cells and chemokine production. Our study reveals alternative mechanisms that explain how cognate antigen suppresses CNS inflammation and may be applicable for effectively and safely treating demyelinating diseases.

INTRODUCTION

Autoimmune demyelinating diseases including multiple sclerosis (MS) affect over two million people worldwide and cause functional and cognitive decline leading to permanent disability and reduced life span (*1*–*3*). MS pathogenesis remains incompletely understood, but current hypotheses based on major histocompatibility complex (MHC) antigen associations and other evidence suggest that peripherally activated central nervous system (CNS) antigen–specific lymphocytes migrate to the brain and spinal cord and coordinate inflammatory reactions. In particular, T cells and other immune cells produce cytokines including interleukin-6 (IL-6), IL-1β, interferon-γ (IFN-γ), and IL-17 and chemokines CCL5, CCL7, and CXCL10 that cause myelin destruction and neurodegeneration (*4*–*7*). This hypothetical mechanism is supported by evidence from the animal models of experimental autoimmune encephalomyelitis (EAE) in which peripheral immunization with CNS-derived protein or peptides causes myelin antigen–reactive CD4$^+$ T cells to infiltrate the CNS resulting inflammation and demyelination (*8*–*11*). Foxp3$^+$ regulatory T cells (T_{regs}) may counterbalance the inflammatory attack through production of anti-inflammatory cytokines such as the transforming growth factor–β and IL-10 (*4*, *5*).

Similar to most autoimmune diseases, the treatments for MS and autoimmune demyelinating diseases are mainly nonantigen-specific immunomodulators such as steroids, IFN-β, fingolimod, dimethyl fumarate, and natalizumab (*12*–*17*). These nonspecific immunomodulators can have serious, sometimes fatal, side effects such as opportunistic infections and progressive multifocal leukoencephalopathy (*12*–*17*). Lymphocyte-depleting therapies have ameliorated EAE and relapsing-remitting MS, suggesting that eliminating encephalitogenic lymphocytes may be therapeutically effective (*18*, *19*). A remarkable long-standing observation in immunology is that administration of an antigen can specifically suppress an immunological reaction against that antigen, even itself is disease-causing. This effect is called antigen-specific tolerance and has been used as a basis for antigen-specific therapy (AST) of diseases involving pathological adaptive immune responses (*20*). Although it can be effective, such as in preventing inhibitory antibodies in protein replacement therapy in hemophilia, extensive preclinical and clinical testing of AST has not achieved widespread success (*20*). We have a long-term program to study the induction of AST by using intravenous (IV) antigen administration to suppress the function and induce apoptosis of disease-causing T cell clonotypes (*21*, *22*). The induction of cell death is an attractive form of AST because it would permanently eliminate the pathogenic lymphocytes and create a more enduring tolerance and therapeutic effect (*23*, *24*). Our goal is to gain additional insight into how IV antigen administration can change immune parameters to better understand how to increase clinical efficacy of this approach.

There is an extensive literature investigating the concept of AST for MS with a major focus on tolerizing T cells by administering antigen in the absence of costimulation (*20*, *25*–*28*). T cells in some patients with MS recognize several myelin antigens including myelin basic protein (MBP), proteolipid protein (PLP), and myelin oligodendrocyte glycoprotein (MOG), suggesting that these could be potential MS therapeutic antigens, which we will refer to herein as "therigens" (*29*, *30*). Previous work has shown that these antigens can induce EAE and then be used successfully to induce AST and ameliorate EAE (*22*, *31*–*36*). However, some papers indicate that single IV dose of antigen can exacerbate disease (*35*, *36*). Therefore, understanding the physiology of therigen presentation

[1]Molecular Development of the Immune System Section, Laboratory of Immune System Biology National Institute of Allergy and Infectious Diseases, National Institutes of Health, Bethesda, MD, USA. [2]Institute of Immunology, Third Military Medical University (Army Medical University), Chongqing, China. [3]MoE Key Laboratory for Biomedical Photonics, Britton Chance Center for Biomedical Photonics, Wuhan National Laboratory for Optoelectronics, Huazhong University of Science and Technology, Wuhan, Hubei 430074, China. [4]Neuroimmunology Branch, National Institute of Neurological Disorders and Stroke, National Institutes of Health, Bethesda, MD, USA. [5]NIAID Clinical Genomics Program, National Institute of Allergy and Infectious Diseases, National Institutes of Health, Bethesda, MD, USA.
*Corresponding author. Email: lenardo@nih.gov (M.J.L.); lzheng@niaid.nih.gov (L. Z.); wuyuzhang@tmmu.edu.cn (Y.W.); czyzzh@mail.hust.edu.cn (Z.Z.)
†These authors contributed equally to this work.

on antigen-presenting cells (APCs) and the changes in immune parameters during AST is important for designing a safe and effective AST approach to MS and other human demyelinating diseases.

In this study, we created MMPt (myelin oligodendrocyte glycoprotein, myelin basic protein and proteolipid protein, truncated), a therigen or therapeutic protein that contains the most common encephalitogenic antigens from MOG, MBP, and PLP to study AST. We hypothesize that MMPt processing can yield therigens that, when properly presented, can specifically suppress disease-causing T cells in CNS demyelinating diseases. We use intravital microscopy and analysis of cells and cytokines to elucidate several previously unknown aspects of immunity in the CNS including the role of perivascular F4/80$^+$ cells as APCs for therigens. We also show how MMPt reduces T lymphocytes, other inflammatory cells, and the cytokine milieu. These studies help provide a scientific basis for developing antigen-specific therigen immunotherapy for human autoimmune demyelinating diseases.

RESULTS

MMPt fusion protein induces T cell death, tolerance, and amelioration of EAE

The membranous layers of the myelin sheath harbor the proteins MBP, PLP, and MOG that contain antigenic epitopes that are recognized by immune responses in patients with MS, which can either cause EAE in experimental animals or induce tolerance and ameliorate EAE (Fig. 1A) (*37*–*39*). We created a polyprotein MMPt of large antigenic portions of these proteins by splicing a truncated portion of the extracellular domain of MOG (amino acids 31 to 152) onto a previously reported protein fusion of MBP and portions of PLP, termed MP4, that can be used to induce EAE as well as a potent AST for MBP or PLP-induced EAE (Fig. 1B) (*40*, *41*). MMPt contains a collection of the most common encephalitogenic antigenic epitopes identified in MS that could serve as therigens (*29*, *30*). We purified MMPt to near homogeneity as a well-defined protein species for IV injection (Fig. 1C). As an in vitro test, we challenged activated T cells derived from $MOG_{35–55}$ peptide ($MOGp_{35–55}$)–specific 2D2 T-cell-receptor (TCR)–transgenic (Tg) mice with MMPt presented on irradiated splenocytes and found that it could induce dose-dependent death of the cells (fig. S1A). Cell death in this experiment required antigen-specific engagement because the MOG-responsive 2D2 T cells died in response to MMPt and MOGp alone but not ovalbumin (OVA) or MP4 (fig. S1A). A control experiment using an anti-TCR agonist, anti-CD3, showed that activated T cells in the preparation died from TCR engagement (fig. S1B). Thus, MMPt is antigenically active. This antigen induced specific T cell death present with specificity and typical dose- and time-dependent loss of viable cell counts (fig. S2).

We next tested whether MMPt could be used as AST in vivo. Protein antigens administered intravenously without costimulation have been shown to induce tolerance (*42*). Therefore, we treated more than 10 mice in replicate experiments for each group with IV administration of MMPt in monophasic and relapsing-remitting EAE (RR-EAE) mouse models (fig. S3, A and B) (*8*, *43*). In the monophasic model, control mice developed an average of grade 3 EAE disease with severe hind limb paralysis and compromised mobility around day 15 and did not recover motor function by day 20 (Fig. 1D). By contrast, 400 μg twice a day or 800 μg once a day of MMPt IV injections on days 7, 9, and 11, right before the disease onset, completely prevented paralytic disease (Fig. 1D and fig. S3A). To model a clinical situation in which an affected patient is seeking treatment, we administered MMPt near the peak of clinical signs on days 14, 16, and 18 of the EAE induction. We observed that this treatment greatly improves motor deficits in EAE mice (Fig. 1E and fig. S3A). Thus, MMPt has both preventive and therapeutic effects on MOG-induced disease. To observe the treatment effect more carefully, we recorded videos of treated individual EAE mouse. We observed that MMPt achieved a very rapid recovery with obvious improvement after two treatment doses (400 μg × 2 times/day) in less than 24 hours and nearly complete restoration of motor function after six treatment doses over the course of 5 days (fig. S3A and movie S1). Overall, the treatment works quickly to reverse severe paralytic disease in EAE mice.

Since most MS therapeutics are approved for relapsing-remitting disease, we also investigated a relapsing-remitting mouse model (fig. S3B). We found that MMPt treatment on days 12, 14, and 16 during the first wave of disease could reduce the clinical score and disease relapse (Fig. 1F). Similarly, MMPt administration on days 18, 20, and 22 during disease remission could significantly reduce the relapse severity (Fig. 1G). These treatment effects were evident in histopathological sections showing a marked decrease in cell infiltrate. Specifically, hematoxylin and eosin staining showed reduced mononuclear infiltration (fig. S4), and toluidine blue and Luxol fast blue/periodic acid–Schiff staining showed less demyelination following MMPt treatment (fig. S5). We also examined multifunctional effects of therigens on treating epitope-spread involved pathogenesis in EAE and found that MP4, a fusion protein composed of MBP and PLP but not MOG, could significantly alleviate MOGp immunogen–initiated EAE in mice (fig. S6). Moreover, MMPt exhibits significant preventive and therapeutic effects on mouse EAE induced by mouse spinal cord homogenate, a mixture of all myelin-encephalitogenic immunogens (fig. S7). Thus, IV MMPt is a highly effective therigen that can reverse clinical disease and CNS pathology.

Supporting the concept of antigen specificity in a model unrelated to EAE, we found that an $OVA_{323–339}$ peptide (OVAp), but not equivalent amounts of an irrelevant peptide, caused in vivo death of activated OVAp-specific TCR-Tg T cells, and vice versa, MMPt can only selectively deplete $MOG_{35–55}$ peptide–specific TCR-Tg T cells in vivo (fig. S8, A and B). We also tested whether T cell death is sensitive to cyclosporin A (CsA), a strong inhibitor of T cell activation and cytokine production. We were surprised to find while being capable of efficiently inhibiting T cell activation and proliferation, CsA does not prevent antigen-driven T cells deletion; moreover, it exhibits little effect on MMPt treatment in MOGp-induced EAE (fig. S8, C and D) (*44*).

Antigen shows rapid distribution in vivo

To understand how MMPt exerts a therapeutic effect, we examined the uptake of rhodamine-conjugated MMPt protein (R-MMPt) versus rhodamine-conjugated chicken OVA (R-OVA) control after IV injection in the CNS and other organs in normal and EAE mice at the peak of monophasic disease. Three hours after injection, the two antigens were largely distributed similarly in organs, especially in the liver, but R-MMPt was enriched in the lungs, whereas R-OVA predominated in the kidneys (Fig. 1, H and I, and fig. S9). Uptake of both R-MMPt and R-OVA was identical in the brain, spinal cord, and leptomeninges by either tail vein

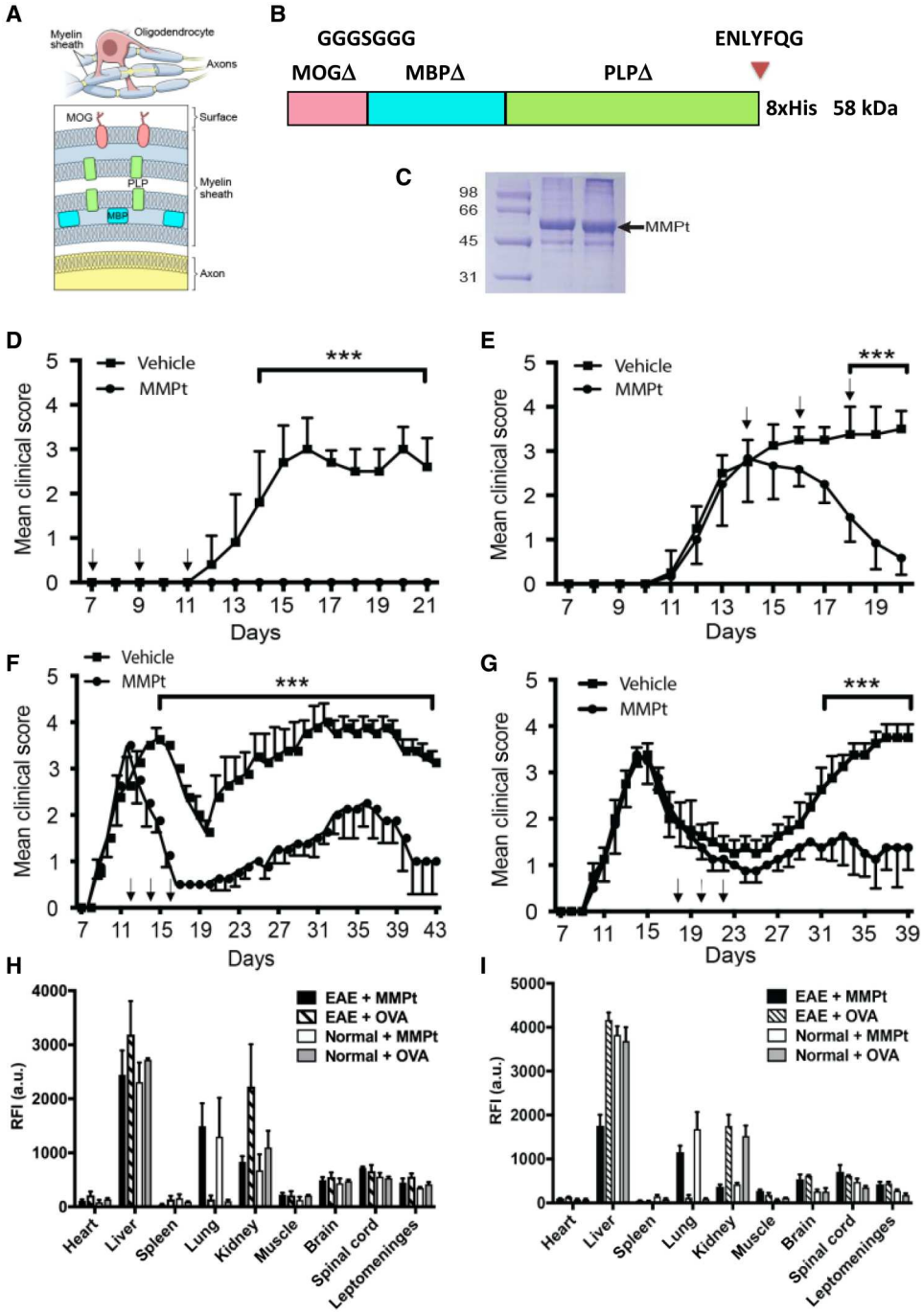

Fig. 1. Characteristics of MMPt as a multivalent therigen that can suppress EAE. (**A**) Diagram of encephalitogenic myelin protein distribution in neuron axon myelin sheath, showing the anatomy of the oligodendrocyte and myelin sheath on axons (top) and cross section of the myelin sheath displaying the relative locations of MOG, MBP, and PLP (bottom). (**B**) Schematic presentation of MMPt antigenic therigen. The human MOG, MBP, and PLP with hydrophobic domains removed (delta) are fused to the TEV cleavage site (ENLYFQG) and a histidine tag at the C terminus. (**C**) Coomassie Blue–stained gel electrophoresis result showing purified MMPt at the expected molecular weight migration (58 kDa). Molecular weight standards at the left. (**D** to **G**) Mean clinical disease scores versus time (days) with various regimens of IV administration of 400 μg of MMPt twice daily in MOGp-induced C57BL/6 EAE mice (D and E), and MOGp-induced relapsing-remitting EAE (RR-EAE) in (C57b/6xSJL) F1 mice (F and G). Vertical red arrows indicate treatments by time in days, $n = 4$ in each group. Data represent at least three independent experiments for each panel. Two-way analysis of variance (ANOVA) with Bonferroni's correction has been used for statistical analysis (shown means + SD); ***$P < 0.001$. Organ distribution and quantification of injected rhodamine-conjugated MMPt (R-MMPt) via tail vein (**H**) or retroorbital plexus (**I**). Relative fluorescence intensity (RFI) was measured at 3 hours after injections with indicated samples. Means and SDs represent data from three independent replicates per group. a.u., arbitrary units.

or retroorbital plexus injection. The relative fluorescence intensity of R-MMPt and R-OVA in the normal or EAE inflamed CNS was comparable. There was little uptake in the heart, spleen, or muscle. Thus, IV therigen can access the brain, spinal cord, and leptomeninges, although a substantial amount is quickly lost in the liver, lung, and kidney.

CNS perivascular mononuclear cells capture and present MMPt to activated T cells in situ

Autoimmune demyelination has been thought to involve different APCs, such as CD11c$^+$ dendritic cells (DCs) that prime myelin–reactive T cells, microglial cells that phagocytose myelin debris, and perivascular macrophages that interact with effector T cells in the leptomeninges (*45*–*47*). The cellular distribution of IV protein antigen therapies in real time has not been previously established but is now possible using intravital two-photon microscopy (IVM), which has been used to document cell trafficking in EAE (*48*–*50*). Therefore, we examined the fate of R-MMPt and R-OVA by IVM using implanted spinal cord window chambers. Using Tg CX3CR1–GFP (green fluorescent protein) mice to visualize the distribution among conventional APCs (DCs and microglia), we observed a rapid perivascular dissemination of the rhodamine-labeled MMPt after IV injection with unexpected late-phase concentration not in CX3CR1$^+$ DC and microglial cells but in an unexpected cell type (Fig. 2 and movie S2). We confirmed this using CD11c-Venus mice to estimate R-MMPt uptake in the conventional DCs and microglia and found no uptake of R-MMPt by CD11c$^+$ (Venus) cells (Fig. 2, C and D; fig. S10; and movie S3). We next used ex vivo fluorescence microscopy staining with CD31 to display blood vessel endothelial cells and other markers (Fig. 2, E, F, H, and I). This revealed that R-MMPt uptake was almost exclusively carried out by F4/80-expressing cells outside of, but juxtaposed to, the blood vessels marked by CD31(Fig. 2, H and I). This was not antigen specific and likely due to the route of administration since we found similar results for IV R-OVA (Fig. 2, E and F). We assessed microglia using the transmembrane protein 119 (TMEM119) marker and found no R-MMPt uptake. In addition, CD3$^+$ T cells (red) associated mainly with F4/80$^+$ cells (blue) and only rarely with the TMEM119$^+$ microglia (green) especially in EAE mice after R-MMPt administration (Fig. 2, G and J, and fig. S11A). Pearson coefficient analysis showed colocalization *R* values between T cells, and DCs, microglia, and macrophages are correspondingly 0.21, 0.39, and 0.65, indicating preferential T cell/macrophage interactions. We observed expression of the activation markers MHC-II and intercellular adhesion molecule–1 (ICAM-1) on F4/80$^+$ cells, which was overall more intense following MMPt administration compared to OVA (Fig. 3, A and B, and fig. S11B). Thus, F4/80$^+$ cells are the primary APCs that take up IV protein during EAE, and a disease-specific therigen MMPt induces greater F4/80$^+$:T cell interactions compared to nonspecific antigen OVA, whereas microglia appear to be the major scavengers for cleaning up apoptotic cells within the inflamed CNS. Further investigations using publicly available human single-cell sequencing datasets reveal an adhesion G protein–coupled receptor E1/Ermes regulator 1 (ADGRE1/EMR1$^+$), CD16$^+$, and CD14$^-$ macrophage population (fig. S12), indicating that this uptake and tolerance mechanism may be conserved in humans.

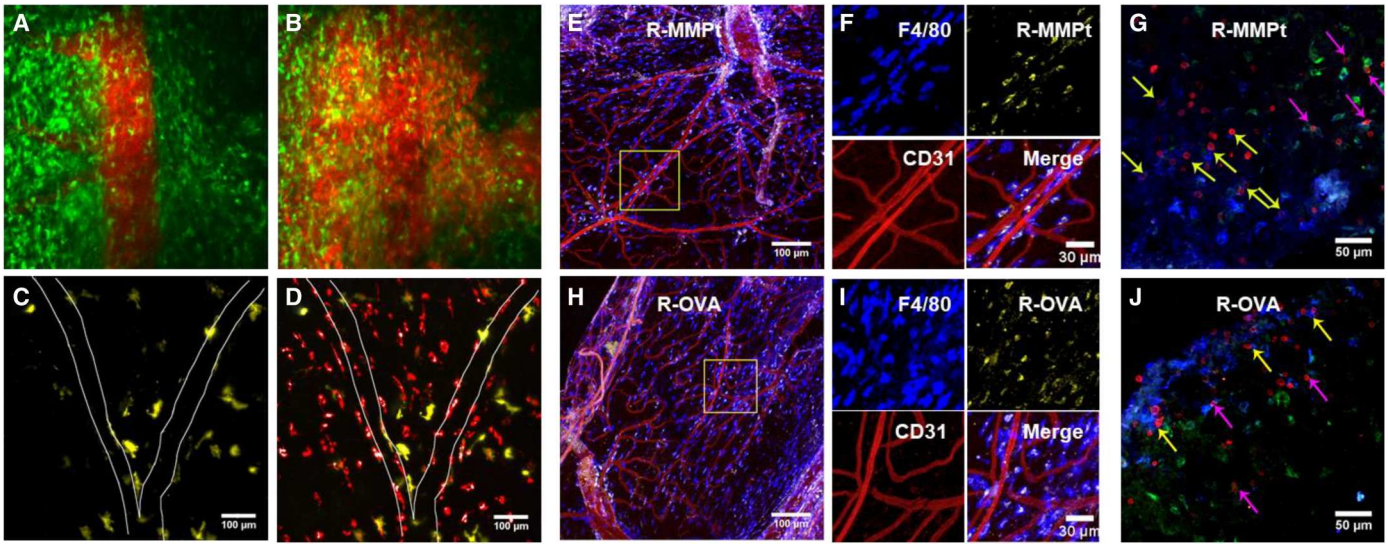

Fig. 2. Perivascular macrophages are the primary therigen-presenting cells in the CNS of C57BL/6 EAE mice. IVM images from different test conditions. (**A**) An intravital confocal image of the spinal cord in CX3CR1-GFP (green) mice immediately after injection of 400 μg of R-MMPt (red). (**B**) As in (A), across blood-barrier distribution of R-MMPt recorded after 30 min. (**C**) The spinal cord in CD11c-Venus (yellow) Tg mice before injection. (**D**) As in (C), 30 min after injection of 400 μg of R-MMPt. (**E** to **H**) Confocal images of axial sections of the spinal cords of EAE mice 3 hours after injection of rhodamine-conjugated proteins are shown as (E), with an injection of 400 μg of R-MMPt (yellow). Scale bar, 100 μm. (F) The inset of (E), indicating macrophages by F4/80 (blue), R-MMPt (yellow), and endothelial mark CD31 (red). Scale bar, 30 μm. (G) Staining F4/80$^+$ macrophages (blue), CD3$^+$ T cells (red), TMEM119 (green). Scale bar, 50 μm. (H) EAE mice received 400 μg IV of rhodamine-OVA (R-OVA, yellow) for 3 hours. Scale bar, 100 μm. (**I**) Inset of (H), with F4/80 (blue), R-MMPt (yellow), CD31 (red). Scale bar, 30 μm. (**J**) R-OVA injection, F4/80-BV421 (blue), CD31–Alexa Fluor 647 (red), and R-OVA (yellow) (E, F, H, and I). Scale bar, 50 μm. For (G) and (J), CD3–Alexa Fluor 594 (red), and TMEM119–Alexa Fluor 488 (green). Yellow arrows, T cells coincident with F4/80$^+$ macrophages; pink arrows, T cells coincident with TMEM119$^+$ microglia. Data represent two independent experiments.

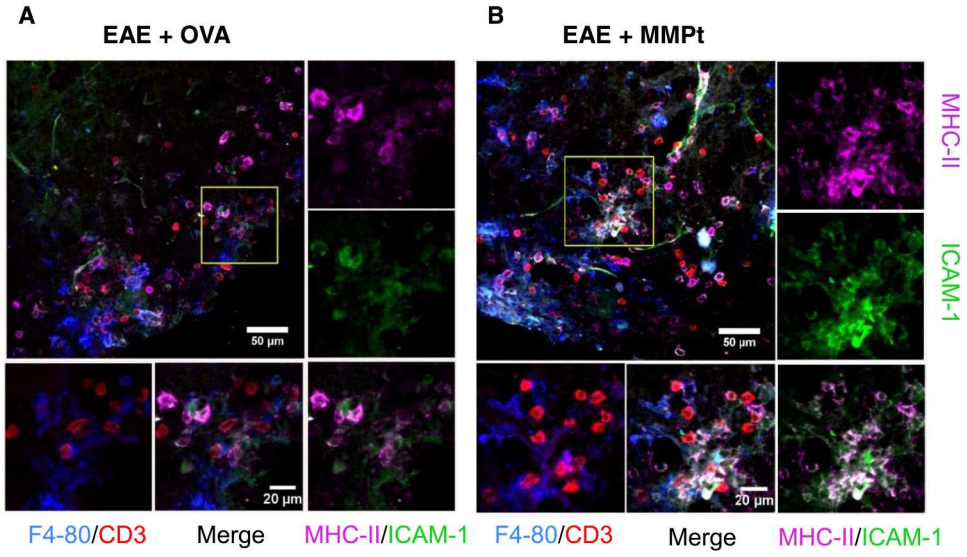

Fig. 3. MMPt up-regulates MHC-II and ICAM-1 expression in macrophages for T cell therigen cross presentation in the CNS of MOGp-induced C57BL/6 EAE mice. Fluorescent microscopic images of axial sections of the mouse spinal cords with a clinical score of 3 EAE. Staining: F4/80$^+$ macrophages in blue, CD3$^+$ T cells in red, ICAM-1 in green, MHC-II in magenta, and ICAM-1 and MHC-II merge as indicated. Post-IV injection of 500 μg of (**A**) OVA or (**B**) MMPt for 3 hours, with ×20 magnification. Scale bars, 50 μm. The insets are presented on individual color and merged channels as indicated flanking on the right and bottom of each representative images at ×40 magnification. Scale bars, 20 μm.

The therigen induces cellular changes in the spinal cord of EAE mice

After determining that perivascular F4/80$^+$ cells consume IV MMPt, we examined the cellular kinetics of T cell engagement by the antigen laden F4/80$^+$ APCs. Previous live imaging of lymph nodes shows that antigen-specific T cells and DC interactions are prolonged by antigen stimulation (*51*). Correspondingly, using IVM in the thoracic spinal cord in EAE mice, we observed that MMPt administration halted migration of GFP$^+$ endogenous T cells within 1 hour (Fig. 4, fig. S11A, and movie 3). Moreover, the in situ appearance of the T cells in OVA or vehicle-treated mice looked large and blast-like, but in MMPt-treated mice, the T cells had a shrunken, apoptotic-looking appearance (Fig. 4, A, C, and E). These T cells showed greater mobility arrest and longer intimate contacts with macrophage-like APCs around blood vessels after MMPt but not OVA administration (Fig. 4, B, D, and F). Quantifying the cellular kinetics of the T cells in situ in mice given IV MMPt showed decrease in cell sizes as a sign of apoptosis (Fig. 4G), overall reduction in velocity, and increased arrest coefficients (Fig. 4, H and I). By contrast, no significant difference was observed in T cell migration, velocity, or arrest coefficient between normal saline and OVA-injected controls (Fig. 4, H and I). Thus, the shrunken, immotile T cells are specific to encounter with F4/80$^+$ cells laden with MMPt.

MMPt selectively depletes MOG-specific effector T cells and tissue-resident memory T cells

Restimulation of activated and cycling T cells through their TCR can induce cell death, particularly following strong antigen stimulation (*22*, *23*). We therefore hypothesized that the antigen-driven T cell immobilization and cellular shrinkage response were a prequel to death of the activated, apoptosis-sensitive T cells in the CNS lesions during EAE. We therefore induced EAE in CX3CR1-GFP mice and treated them with MMPt or OVA. Using terminal deoxynucleotidyl transferase–mediated deoxyuridine triphosphate nick end labeling (TUNEL) staining, we observed substantially apoptotic cells, especially in the perivascular and meningeal areas after MMPt administration, whereas the TUNEL staining was rarely observable from OVA-treated samples (Fig. 5, A and B). This supports the in vivo IVM observation that the antigen-induced T cell shrinkage leads to apoptosis (Fig. 4). We also observed TUNEL-stained cell fragments in the spinal cord parenchyma coincident with CX3CR1$^+$ microglia after MMPt but not OVA treatment. We postulated that these apoptotic cells within microglia were apoptotic T and other infiltrating cells that had been phagocytosed. To test this hypothesis, we performed an adoptive transfer experiment. Activated $MOG_{35–55}$-specific 2D2-TCR-Tg T cells were labeled with Dye 670 and injected during EAE induction. These mice were treated with MMPt and evaluated for apoptotic cell engulfment by ex vivo microscopy on the spinal cords immersed in phosphate-buffered saline (PBS). We directly visualized increased amounts of Dye 670 fragments within CX3CR1$^+$ cells, indicating that microglia were clearing out the apoptotic T cell debris (Fig. 5C).

The observation of specific therigen-induced T cell apoptosis in the affected CNS suggests that spinal cord disease–infiltrating T cells will be reduced by MMPt treatment. Hence, we isolated mononuclear cells after spinal cord dissection and quantified cell populations by flow cytometry. Compared to the vehicle controls, MMPt caused a progressive dose-dependent depletion in CD3$^+$CD45$^+$ T cells at days 15 and 20 of EAE (Fig. 5, D and E). Correspondingly, the MMPt notably increased annexin V staining in CD3$^+$ T cells, further confirming that the therigens caused antigen-induced T cell apoptosis in situ (Fig. 5F). We were surprised to also observe that MMPt reduces rare CNS-resident memory CD69$^+$CD11a$^+$ tissue-resident memory T (T_{RM}) cells (Fig. 5, G and H). Together,

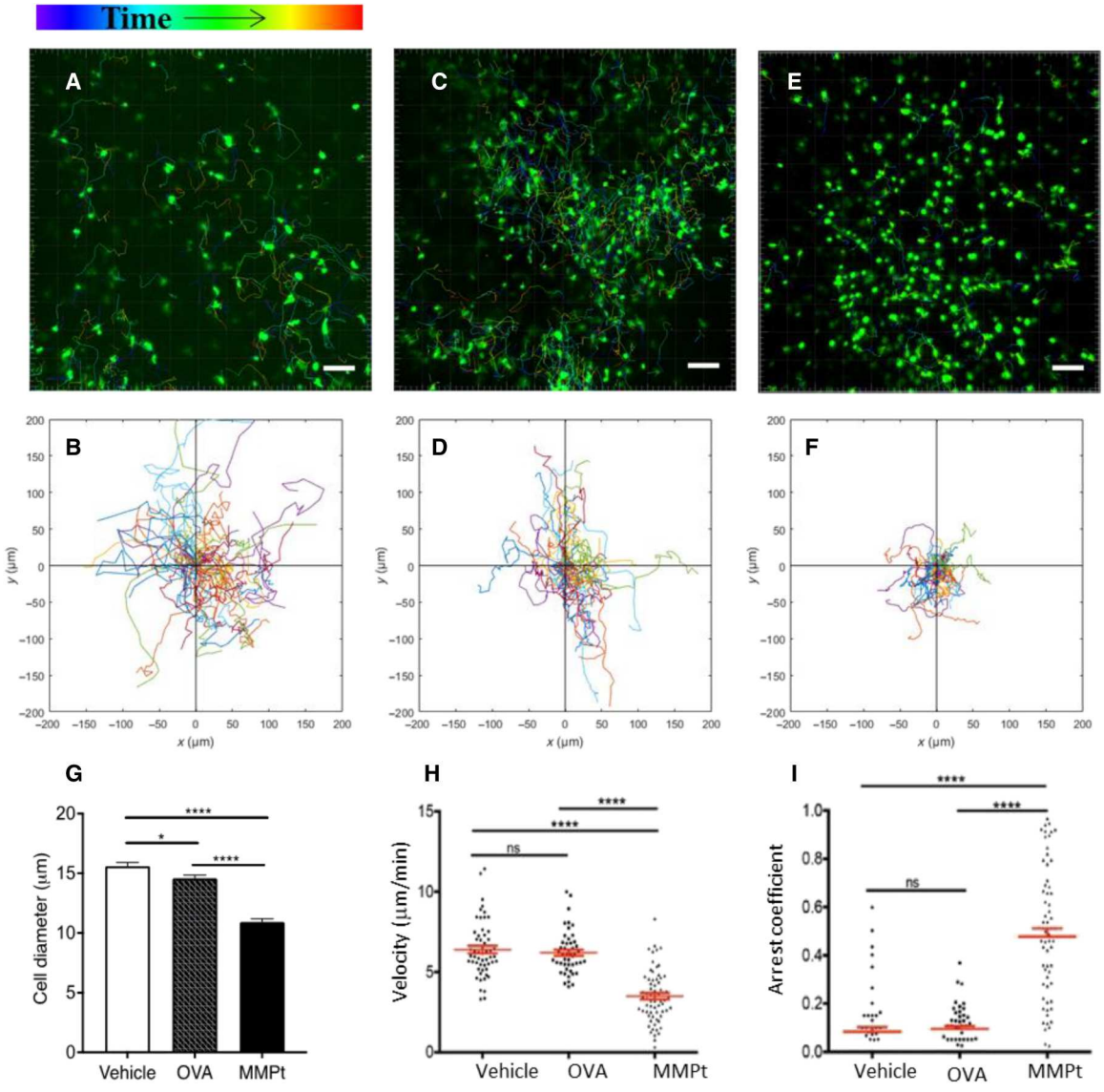

Fig. 4. MMPt-loaded macrophages arrest reactive T cells in the CNS of MOGp-induced, CXCR6-GFP-Tg, and C57BL/6 EAE mice. Intravital microscopic imaging analysis on responses of the encephalitogenic T cells with therigen-loaded APCs in the CNS of EAE mice. Migration distance and velocity of endogenous CXCR6-GFP$^+$ T cells were recorded for 3 hours after antigen administrations in a clinical score of 3 EAE mice (**A** to **F**). Antigen stimulations: saline vehicle (A and B), OVA (C and D), or MMPt (E and F). The images represent typical observations of T cell displacement view in the field of the spinal cord chamber, with its two-dimensional tracking data correspondingly shown in (B), (D), and (F). Scale bars, 50 μm. Data are representative of 60 to 80 tracked cells from two mice per treatment in two independent experiments. (**G**) Cell size in diameters measured from the retrieved images is presented as group means and SEM (error bars). *P < 0.05 and ****P < 0.001 (one-way ANOVA with Tukey's multiple comparisons). Cell moving velocity data are plotted for showing the migration rate of CXCR6 T cells over the 3-hour courses after injections of vehicle, OVA, or MMPt, as indicated in (**H**). Arrest coefficient of T cells with same parameters as (H) is shown in (**I**). T cell velocity and arrest coefficients were analyzed using two-tailed unpaired t test shown means (red horizontal lines) ± SD (red bars). ns, not significant; ****P < 0.0001.

these data show that clonal deletion of encephalitogenic T cells accompanies the disease-ameliorating effect of MMPt treatment.

MMPt shifts T cell functional profiles to anti-inflammatory in EAE mice

Since motor deficits improved within 24 hours after MMPt treatment, it seemed unlikely to be solely due to suppression of T cell damage and remyelination (Fig. 1 and movie S1). We conjectured that the treatment may also suppress CNS tissue inflammation and therefore examined the effect of MMPt on the inflammatory cytokine milieu. EAE pathogenesis is thought to involve an activation cascade of autoreactive T helper cells 1 and 17 that stimulate innate immune and inflammatory cells to produce cytokines such as IFN-γ, IL-1β, and IL-6 (*52*, *53*). We observed increases in percentage of T_{regs} and IL-10/IFN-γ double-producing T cells in the MMPt-treated EAE spinal cords at the end point of the experiments likely due to a combination of both absolute and relative increases, suggesting their possible role in disease suppression (Fig. 6, A to D, and fig. S13). By contrast, we found no obvious changes in IFN-γ or IL-17 single-producing T cells, although there was a trend to

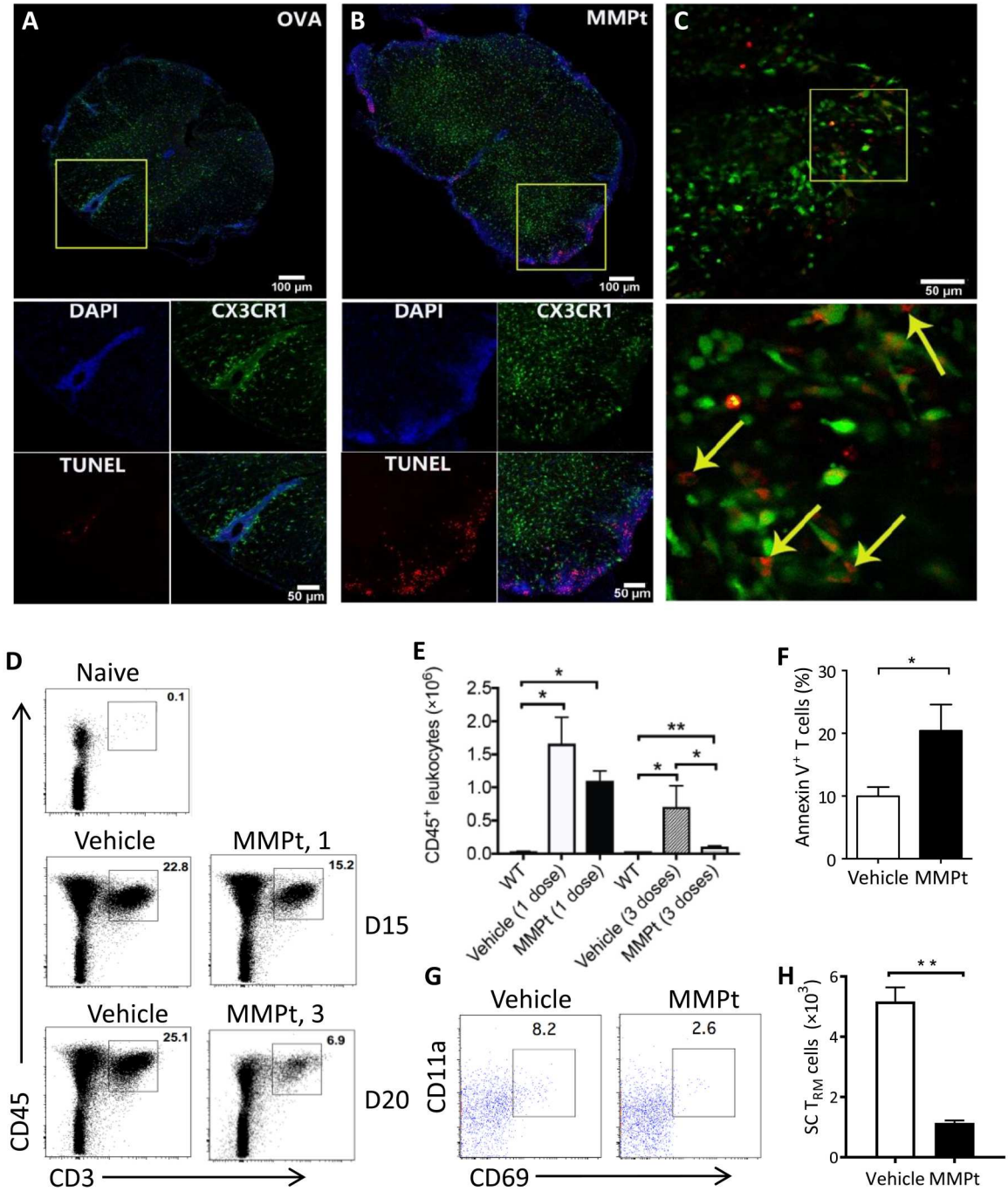

Fig. 5. MMPt induces RICD of the sensitive T cells in blunting inflammatory responses in MOGp-induced C57BL/6 EAE mice. Confocal microscopy imaging with TUNEL staining of axial section of the spinal cords from CX3CR1-GFP-Tg mice with a clinical score of 3 EAE that were IV injected with (**A**) OVA or (**B**) MMPt for 20 hours. Channel presentations are 4′,6-diamidino-2-phenylindole (DAPI; blue), microglia (CX3CR1; green), TUNEL (red). Scale bars, 100 μm (top) and 50 μm (bottom). (**C**) Ex vivo imaging of the spinal cords isolated from CX3CR1-GFP mice at a clinical score of 3 EAE. In addition, 24 hours after MMPt injection, the mice were adoptively transferred with in vitro Dye 670–labeled, activated $MOG_{35–55}$-specific 2D2-TCR-Tg T cells. Scale bars, 50 μm. (Bottom) Inset: A magnification of ×16. Arrows indicate the Dye 670–labeled apoptotic T cell fragments within microglia. (**D**) Frequency of $CD3^+CD45^+$ T cells isolated from the CNS of a clinical score of 3 EAE mice after treatment with one dose (middle) or three doses (bottom) control vehicle or MMPt. (**E**) Quantification of $CD45^+$ leukocytes from (D), average counts of three mice. WT, normal non-EAE mice. (**F**) Annexin V staining of T cells isolated from the spinal cords 24 hours after injection of vehicle or MMPt in mice with an EAE clinical score 3. (**G**) Frequency of $CD69^+CD11a^+$ T_{RM} cells isolated from the CNS of score-3 EAE mice that had received three doses of vehicle or MMPt treatments. (**H**) Quantification of (G) after three doses of vehicle or MMPt, average counts from three mice. Data were analyzed using two-tailed unpaired *t* test (shown means + SD); $^*P < 0.05$ and $^{**}P < 0.01$.

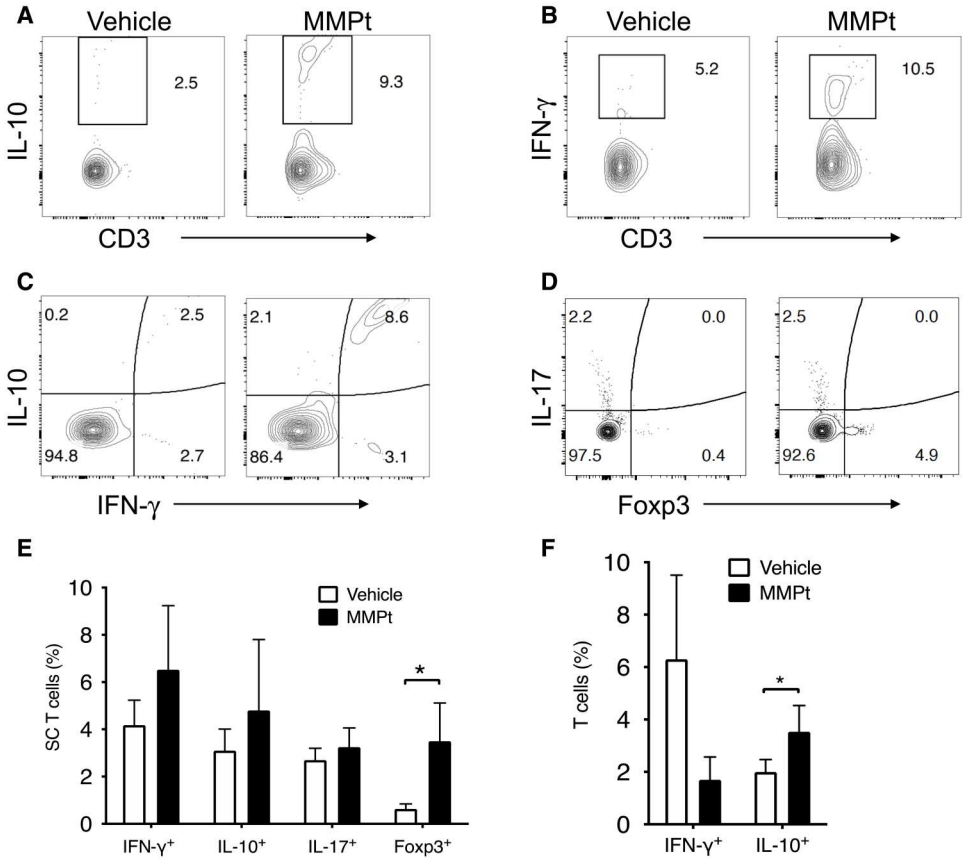

Fig. 6. MMPt induces anti-inflammatory cytokine profiles in the MOGp-induced C57BL/6 EAE spinal cord. Flow cytometry analysis of mononuclear cells isolated from a group of spinal cords ($n = 4$) from EAE mice (clinical score = 3) and stained for the indicated markers. Live cells defined by forward scatter/side scatter (FSC/SSC) were first gated for singlets and subsequently by $CD3^+$ and $CD45.2^+$ for T cells for (A) to (C), and $CD11b^-$ and $CD45.2^+$ T cells for (D) (with gating shown in fig. S12). Analysis of the indicated populations is shown. (**A** to **D**) Frequencies of IL-10^+, IFN-γ^+, IL-17^+, and FoxP3^+ T cells in the EAE CNS of mice that received one dose of IV injection of vehicle or 800 μg of MMPt. (**E**) Frequencies of indicated T cell populations in the spinal cords of EAE mice that received one dose of 800 μg of MMPt treatment for 20 hours. (**F**) Frequencies of IFN-γ^+ and IL-10^+ T cells in the peripheral blood of score-3 EAE mice after three doses of normal saline vehicle or MMPt treatment (800 μg/day). Significance of the cell percentage changes was statistically analyzed using two-tailed unpaired *t* test (shown as means + SD); $*P < 0.05$.

increased IFN-γ producers (Fig. 6E). In the peripheral blood, MOGp-responsive T cells showed reduced IFN-γ and increased IL-10 expressions after MMPt treatment (Fig. 6F). Thus, it appears that eliminating antigen-specific T cells and inflammatory cells modulated the inflammatory cytokine milieu. We further examined the effect of MMPt on cytokines, particularly those responsible for innate immune responses within the affected CNS. Using quantitative polymerase chain reaction (PCR) to measure cytokine mRNA, we found that one dose of MMPt reduced the high expression of IFN-γ, IL-1β, and IL-2Rα but not IL-18 mRNA (Fig. 7A). In further studies, we found that repeated doses of MMPt caused reductions in innate immune cells. We found that within 20 hours of MMPt treatment, there was a reduction in the frequency and absolute number of microglia ($CD11b^+CD45^{int}$), infiltrating myeloid DCs ($CD11b^+CD45^{hi}CD11c^+$), macrophages ($CD11b^+CD45^{hi}CD11c^-Ly6G^-$), and neutrophils ($CD11b^+CD45^{hi}CD11c^-Ly6G^+$) (Fig. 7, B and C), among which the MMPt-induced apoptosis of CNS-infiltrating macrophages appears to be prominent (fig. S14). In addition, we found that chemokines responsible for immune cell recruitment such as CCL5, CCL7, CXCL10, and CXCL11 were also reduced (Fig. 7D). The swiftness of these changes after MMPt administration appears to explain rapid disease amelioration.

DISCUSSION

AST approaches based on natural endogenous immunoregulation have been long-sought as an adjunct to general immunosuppressants for treating autoimmune diseases due to autoreactive T cells (*16*). Antigen-specific T cell apoptosis, called restimulation-induced cell death (RICD), is a general mechanism for homeostatic control of the immune system, and we have advocated this mechanism as a basis for AST (*22*, *40*). It would be ideal for treating autoimmune diseases where pathogenic antigen epitopes are identifiable, unvarying, and selectively delete specific disease-causing T cells. We have previously shown that myelin encephalitogenic antigens can eliminate specific T cells and alleviate EAE in experimental animals (*31*, *41*). Here, we demonstrate that MMPt, a fusion protein containing the major myelin encephalitogenic epitopes, can induce apoptosis of the disease-causing T cells in the inflamed CNS. We show that this induction of T cell inactivation and apoptosis occurs directly in situ in the spinal cord in response to antigen. Associated with

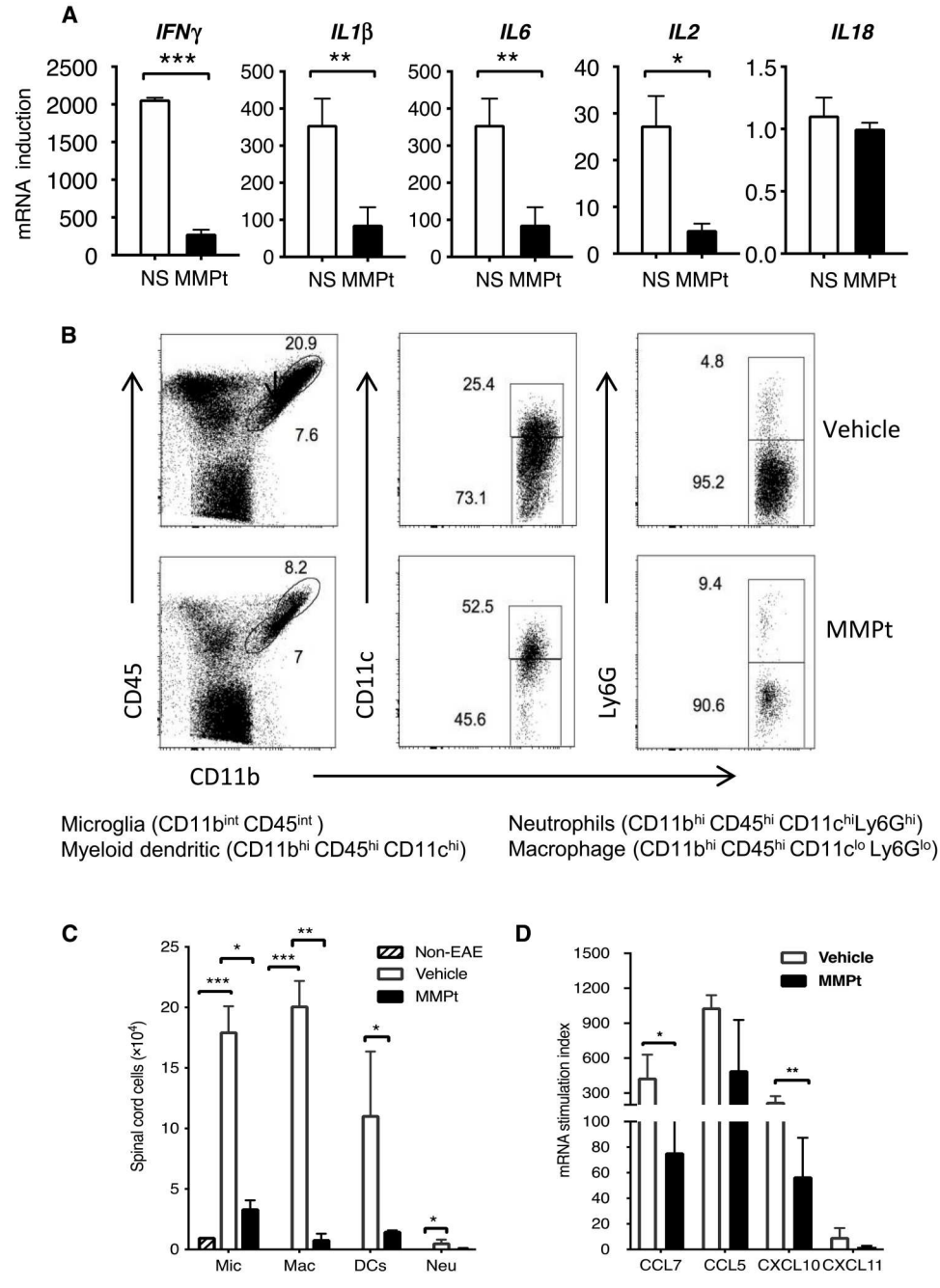

Fig. 7. MMPt-induced T cell depletion leads to suppression of inflammatory cytokines in the CNS of MOGp-induced C57BL/6 EAE mice. (**A**) Quantitative PCR results for indicated cytokines from the spinal cord mononuclear cells isolated from mice of day 20 post-EAE induction that were treated at day 14 of disease scoring of 3 with IV injections of one dose of 800 μg of MMPt or normal saline (NS) control. (**B**) Frequency of microglia (Mic), myeloid DCs, macrophages (Mac), and neutrophils (Neu) in the affected CNS of mice that received three doses of vehicle control or 800 μg of MMPt every other day starting from day 14 of EAE induction that presented with a disease score of 3 is shown with gating, and each specific population is specified at the bottom. (**C**) Quantification of (B) with absolute cell counts on average of three mice per group. (**D**) mRNA stimulation index derived from quantitative PCR data measuring expression of chemokines of EAE CNS tissue isolated from EAE mice that received one dose of IV injection of normal saline or 800 μg of MMPt for 20 hours. Data were analyzed using two-tailed unpaired *t* test (shown means + SD); **P* < 0.05, ***P* < 0.01, and ****P* < 0.001. Data represent two independent experiments.

this is a rapid resolution of inflammation as well as peripheral deletion of antigen-specific T cells. These effects and possibly other tolerogenic effects, such as T_{reg} induction, could be beneficial for improving the symptoms of immune-mediated demyelinating disease.

Further exploration on the underlying mechanisms of therigen treatment reveals interesting discoveries. Unexpectedly, MMPt uptake is mainly by the perivascular F4/80$^+$ cells rather than CD11c$^+$ DCs or microglia, which might have been expected from previous studies (*45*, *46*, *54*–*56*). We found that the meningeal F4/80$^+$ cells in the inflamed area have up-regulated ICAM-1 and MHC-II associated with the death of MOGp-specific T cells (Fig. 5 and movie S2). Another key observation is that MMPt did not cause cytokine "storm." Inflammatory cells, cytokines, and chemokines were markedly reduced. Thus, MMPt is an effective and safe tolerogenic therigen for established CNS inflammation. CNS-resident macrophages, DCs, and microglial cells have all been previously implicated as functional APCs for antigen presentation in demyelinating diseases (*45*, *46*, *54*–*56*). Depletion of perivascular macrophages causes a decrease in EAE symptoms, suggesting importance of macrophages in causing CNS inflammation (*57*–*59*). Recent studies have further elaborated the complexity of origin and biological functions of these macrophages (*60*, *61*). Live imaging of the peripheral lymph nodes showed that immunogen presentation relies on interactions between T cells and DCs (*51*). Conversely, others claim that DCs also function as tolerance-inducing APCs in the CNS (*62*). Our data show that T cell deletional tolerance is associated with prominent antigen uptake in perivascular F4/80$^+$ cells, suggesting that these resident macrophages likely play a key role in therapeutic antigen presentation in the CNS. The F4/80 antigen, first identified by Austyn and Gordon, is expressed in various mouse mononuclear populations, including tissue macrophages, macrophages of T cell areas, and marginal zone in lymph nodes, lung alveolar macrophages, and classical DCs (*63*). More recent exciting studies in high-dimensional single-cell mapping using mass cytometry showed that F4/80 was highly expressed on CD206$^+$ CD38$^+$ border–associated macrophages and the most numerous leukocytes isolated from the brain were shown to be distinct from microglia. In addition, F4/80 was observed on eosinophils, monocytes expressing variable amounts of Ly6, and other rare microglia and monocyte-derived cells (*64*, *65*). Other studies suggest that border-associated or perivascular macrophages are derived from blood-borne monocytes and are capable of phagocytosing material in the perivascular space (*66*). The physiology of CNS tolerance induction in EAE appears to be a complex interplay of essential populations of cells in the CNS, for which F4/80$^+$ perivascular cells act as primary APCs, while T cells are powerful inducers of the inflammatory response, and CD11c$^+$ DCs together with macrophages seem to govern cytokine release (*67*). In addition, microglial cells phagocytose apoptotic T cells and scavenge debris in EAE (*68*).

The deletion of MMPt-sensitive T cells, including the activated effector T cells and resident T_{RM} cells, appears to be permanent, as T cells isolated from MMPt-treated EAE mice failed to respond to MOG stimulation ex vivo. MMPt treatment at the first disease peak provides extended protection against a second EAE flare. The clinical improvements happening less than 1 day after MMPt treatment were found to correlate to death of disease-causing T cells, along with a robust suppression of the innate immune inflammation, including elimination of infiltrating macrophages and resident microglia and DCs and neutrophils, as well as IFN-γ, IL-1β, IL-6, CCL5, CCL7, CXCL10, and CXCL11. These changes would strongly blunt the inflammatory processes of EAE (*69*). However, further studies are necessary to clarify if this depletion of antigen-specific T cells directly leads to the collapse of local inflammation due to monocyte apoptosis or involves other important mediators, such as T_{regs}.

One of the principal challenges in demyelinating disease is antigen selection. MMPt is composed of the hydrophilic portions of MOG, MBP, and PLP against which T cell responses have been demonstrated in MS (*10*, *27*). However, individual peptides selected from these proteins have shown only limited success in treating patients with EAE and MS (*70*). Nevertheless, our approach enables an individual set of antigens to be selected by the host system during initial disease and in response to potential epitope spreading in more advanced disease (*37*, *41*, *71*, *72*).

The clinical response to MMPt is the most marked when given in a monophasic EAE model. While tested in a mouse relapsing remitting EAE model, MMPt can significantly reduce the severity but is unable to eliminate the clinical motor deficits during the relapse. The mechanism underlying the incomplete protection is unclear, as there are several possible explanations. First, the relapsing-remitting model may involve more T cell clones sensitive to epitope-spreading myelin antigens beyond MMPt coverage. Second, there is a continuous replacement of newly matured thymocytes in the periphery that are continuously activated by existing EAE induction. Last, the disease may involve neuroinflammation and neurodegeneration resulting in deficits that may resolve only with an extended healing process or not at all. The inability of MMPt to fully eliminate relapses implies that a tolerogen approach to MS treatment would be best deployed during early development of the disease with less burdens from demyelinating lesions.

This study provides evidence demonstrating that AST is effective and safe in treating EAE in mice. While our data suggest antigen-specific depletion, further comparison of multiple antigen-specific T cells and its effect on controlling autoimmune inflammation is required to establish this point definitively before translational medical trials, for which we could also benefit from further advancement of our knowledge on the multifactorial steps involved in the physiological effects of tolerogen administration in EAE models, along with encouraging advanced technologies that may considerably improve spatiotemporal therigen delivery in vivo. The medical translatability to humans is not established in our study, but we believe that the statistically significant preventative and therapeutic effect of MMPt in the spinal cord homogenate experiment is encouraging. It is important because we did not tailor the disease-inducing antigens in any way to the treatment antigens as is often done to show tolerance effects in mouse experiments. While we agree that it would be premature to draw conclusions about human disease without a clinical trial, we think that these results are hopeful. For example, a partial treatment effect reducing spinal cord inflammation as we have demonstrated would not completely cure the disease but might prevent progression from difficulty walking to being wheelchair bound. On the basis of these encouraging data, we are investigating strategies to improve the chances of success, such as screening with the polyprotein for reactivity by a new type of blood test so that only patients that have existing reactivity would receive treatment. In addition, route, dose, and frequency of administration may greatly affect the efficacy in

humans. Last, currently available biological therapies have a wide range of efficacy in different patients. Since the antigen-specific approach uses a fundamentally different mechanism than current therapies, it is possible that combination therapies would achieve greater efficacy.

MATERIALS AND METHODS

Development and preparation of MP4 and MMPt

The MP4 preparation has been described previously (*41*). We added the truncated extracellular domain of MOG (amino acids 31 to 151 of National Center for Biotechnology Information protein database: Q16653) to MP4 for creating a new polyprotein termed MMPt. This polyprotein contains a comprehensive collection of known and potential MS epitopes separated from a purification tag of 8× histidine by a tobacco etch virus (TEV) cleavage site (ENLYFQG) (Fig. 1B) (*31*). We produced MMPt in *Escherichia coli* as a nonglycosylated protein that we purified to a single band of 58 kDa (Fig. 1C). Mass spectrometry confirmed the band and showed that the faster migrating species were proteolytic degradation products that occurred in minor quantities. The pET-MMPt was constructed by sequential fusing of bacterial codon-optimized cDNA coding sequences for the engineered human $MOG_{31–151}$ amino acid coding sequence) with the full-length 21.5-kDa MBP and the transmembrane domain–truncated PLP proteins. A TEV cleavage site and an 8xHis tag were added at the C terminus of the fusion protein. The *E. coli* strain BL21 Star (DE3) was used for transformation, and a selected single clone was used for preparative fermentation using 500 ml of Overnight Express System medium (Novagen) in a 4-liter Erlenmeyer flask, shaking at 250 rpm at 37°C until optical density at 600 nm reached 2.5. Cell pellets were stored at −20°C overnight. Pellets were resuspended in tris buffer [50 mM (pH 8.0)] containing complete protease inhibitor (Roche) and disrupted via sonication. Last, the insoluble material was collected by centrifugation at 24,000 rpm for 20 min, and the supernatant was discarded. Insoluble pellets were resuspended in 100 ml of extraction buffer [8 M urea, 40 mM imidazole, 0.5 M NaCl, 20 mM sodium phosphate, and 5 mM β-mercaptoethanol (pH 7.4)] via sonication and vigorous trituration. The mixture was centrifuged at 24,000 rpm for 15 min, and the supernatant was immediately put on ice. The extraction step was repeated five times to ensure the full recovery of MMPt from insoluble pellets, and the combined supernatants were filtered through a 0.22-μm Millipore Express PLUS membrane. After filtration, the sample was applied to a 5-ml HisTrap HP column (GE Healthcare) and washed with at least 5 column volumes of the extraction buffer. The column was subsequently washed with 50 column volumes of buffer A [0.1% Triton X-114, 8 M urea, 40 mM imidazole, 0.5 M NaCl, 20 mM sodium phosphate, and 5 mM β-mercaptoethanol (pH 7.4)] and 10 column volumes of the extraction buffer at 4°C. To elute MMPt, 5 ml of buffer E [8 M urea, 500 mM imidazole, 0.5 M NaCl, 20 mM sodium phosphate, and 5 mM β-mercaptoethanol (pH 7.4)] was applied to the column while monitoring optical density at 280 nm (Fig. 4). Additional β-mercaptoethanol was then added to the elution fraction to bring up the concentration of the reductant to 50 mM. MMPt was subsequently applied to a 1 cm–by–25 cm length C4 Vydac reversed-phased high-performance liquid chromatography column equilibrated in 65% solvent B (1:1 formic acid:H_2O) and 35% solvent C (1:1 acetonitrile:formic acid) with a flow rate of 4.0 ml/min. The bound MMPt was eluted with a linear gradient of solvent C (35 to 90%) and lyophilized.

Mice and EAE induction

We purchased C57BL/6, (C57BL/6xSJL) F1, 2D2-TCR-Tg, and DO11.10-TCR-Tg mice from the Jackson Laboratory. Mice were maintained in a specific pathogen–free facility and used under protocols approved by the National Institute of Allergy and Infectious Diseases (NIAID) Animal Care and Use Committee (protocol LISB-7E). EAE was induced by immunization of female C57BL/6 mice (10 to 12 weeks old) with 200 μl of emulsion containing 100 μg of $MOGp_{35–55}$ and 400 μg of *Mycobacterium tuberculosis* extract H37 Ra (Difco) in Freund's complete adjuvant (FCA) as previously described (*73*). At 4 and 24 hours after immunization, mice received 200 ng of pertussis toxin (List Biological Laboratories) intraperitoneally. To induce RR-EAE in (C57BL/6xSJL) F1 mice, we immunized the female F1 mice with 200 μl of emulsion containing 200 μg of $MOGp_{35–55}$ and 400 μg of *M. tuberculosis* extract H37 Ra (Difco) in FCA. At 4 and 24 hours after immunization, mice received 75 ng of pertussis toxin intraperitoneally. EAE was scored by the methods previously described (*74*, *75*).

For intravital imaging, C57BL/6.Cg-Tg (Itgax-Venus) 1Mnz/J (CD11c-YFP, Research Resouce Identity (RRID): IMSR_JAX:008829) mice, C57BL/6.129P2-$Cxcr6^{tm1Litt/J}$ ($Cxcr6^{+/gfp}$, RRID: IMSR_JAX:005693) mice, and B6.129P2(Cg)-$Cx3cr1^{tm2.1(cre/ERT2)Litt}$/WganJ ($Cx3CR1^{+/gfp}$, RRID: IMSR_JAX:005582) mice were derived from breeding pairs that were originally obtained from the Jackson Laboratory (Bar Harbor, Maine, USA). To generate multicolor-coded Tg mice, CD11c-YFP mice were bred with CXCR6-GFP mice. All the mice were bred and maintained in a specific pathogen–free barrier facility at the Animal Center of Wuhan National Laboratory for Optoelectronics. All animal studies were approved by the Hubei Provincial Animal Care and Use Committee and followed the experimental guidelines of the Animal Experimentation Ethics Committee of Huazhong University of Science and Technology.

Surgical procedure

Optical access to the spinal cord was achieved by means of a single laminectomy at the vertebral T6 level. Briefly, a midline incision of ~1 cm in length was performed on the shaved back of the experimental mouse. The skin was then retracted to expose the muscles and tissues covering the vertebra of interest. Upon removal of the dorsal aspect of the vertebra, the dura mater was carefully removed, and the spinal cord at Th6 to Th11 was surgically exposed as previously described (*76*). Following surgery, the mouse was placed on a custom-made stabilization device on a heating pad maintained at 37°C. After the surgery, mice received 150 μl of sterile saline subcutaneously and were placed in the cage for recovery.

Intravital microscopy

CX3CR1-GFP or CXCR6-GFP/CD11c-Venus mice were anesthetized via inhalation of 1.0 to 3.0% isoflurane in oxygen flow using a Matrix VMS small animal anesthesia machine (Midmark, Dayton, OH, USA). The window was fixed on a warm plate (Thermo Plate) using a custom-made holder and then fastened to the microscope stage. Intravital images were obtained using an LSM780 system. The images were captured using a 20× water immersion objective

(numerical aperture, 1.0). During the intravital imaging process, mice were maintained at 37°C with a warm plate. Confocal Laser Scanning Microscopy (CLSM) was used to simultaneously image the microglial cells or T cells (488-nm laser, 500- to 550-nm emission) and rhodamine-labeled MMPt drugs (561-nm laser, 570- to 620-nm emission) or Dye 670–labeled exogenous T cells.

MMPt treatment

For EAE treatment experiments, 800 μg of MMPt once a day (or 400 μg twice a day with a 6-hour interval), vehicle control (sterile normal saline) was administered by retroorbital IV injection on either days 8, 10, and 12 after MOG immunization (for prevention of clinical motor deficits) or on days 14, 16, and 18 after MOG immunization (for therapeutic intervention after clinical motor deficits develop). For RR-EAE treatment, 800 μg of MMPt once a day was administered by IV injection on either days 12, 14, and 16 (for treatment during the first inflammatory phase) or on days 18, 20, and 22 (for late therapeutic treatment). Each replicate experiment contained five mice per group.

Isolation of CNS mononuclear cells

Mice were euthanized and then perfused through the left ventricle of the heart with PBS. Spinal cords (SCs) were flushed out from the spinal columns with PBS. SC tissues were cut into small pieces and then digested using a neural tissue dissociation kit (Miltenyi Biotec, Germany) to make single-cell suspensions. The digested cells were passed through a 70-μm cell strainer, followed by sucrose (0.9 M in Hanks′ balanced salt solution) centrifugation at 850*g* at 4°C for 10 min. The mononuclear cells were pelleted for further analysis.

Flow cytometry

All flow cytometry antibodies are from eBioscience or BioLegend. For surface staining, single-cell suspensions from the spleen, lymph nodes, SCs, and in vitro expanded T cells were washed with PBS and incubated with surface staining antibodies (1:200 dilution) at 4°C for 30 min in the dark. The cells were then washed with PBS once and then analyzed using an LSRII flow cytometer. For intracellular cytokine staining, cells were prepared as described and stimulated with phorbol 12-myristate 13-acetate (50 ng/ml; Sigma-Aldrich) plus ionomycin (1 μg/ml; Sigma-Aldrich) for 6 hours with monensin added for the last 3 hours (1 μl/ml; BD Biosciences). Cells were then stained for surface markers as described above, fixed and permeabilized using the Fixation and Permeabilization Buffer (eBioscience) according to the manufacturer′s instructions, and incubated with antibodies against cytokines of interest before analysis. We characterized cell subsets in the spinal cord as follows: $CD45^{int}$ $CD11b^{+}$ (microglia), $CD45^{high}$ $CD11b^{+}CD11c^{-}Ly6G^{-}$ (macrophages), $CD45^{high}$ $CD11b^{+}CD11c^{+}$ (DCs), $CD45^{high}$ $CD11b^{+}Ly6G^{+}$ (neutrophils), and $CD45^{high}$ $CD11b^{-}CD3^{+}$ (T cells) (*77*).

Immunofluorescence staining

For the immunofluorescence analysis, spinal cord tissues from $CXCR6^{GFP/GFP}$ and CD11c-Venus heterozygous mice were fixed in 4% paraformaldehyde for 12 hours at 4°C and then dehydrated in 30% sucrose solution for 48 hours. The tissues were then frozen in optimal cutting temperature (OCT) (Sakura, Torrance, CA, USA) compound and sectioned into 20-μm slices using a freezing microtome (Leica, Germany). OCT was removed by washing three times in PBS, and the sections were immunostained with Alexa Fluor 594 anti-mouse F4/80 (clone BM8, BioLegend) for macrophage and Alexa Fluor 647 anti-mouse ICAM-1 (clone YN1/1.7.4, BioLegend) for immune synapse. Other antibodies used in these experiments were as follows: Brilliant Violet 421 anti-mouse F4/80 (1:200; clone BM8, BioLegend), Alexa Fluor 488 anti-mouse ICAM-1 (1:200; clone YN1/1.7.4, BioLegend), Alexa Fluor 594 anti-mouse CD3 (1:200; clone 17A2, BioLegend), Alexa Fluor 647 anti-mouse CD31 (1:200; clone MEC13.3, BioLegend), primary anti-mouse MHC-II (1:400; clone ab15630, Abcam), mouse monoclonal anti-rat immunoglobulin G2b (IgG2b)/IgG2a conjugated to Alexa Fluor 647 (1:1000; clone ab172333, Abcam), primary anti-mouse TMEM119 (1:400; clone ab209064, Abcam), and mouse monoclonal anti-rat IgG H&L conjugated to Alexa Fluor 488 (1:1000; clone ab150077, Abcam). T cell apoptosis was detected by a one-step TUNEL cell apoptosis detection kit (C1089, Beyotime, China). All the sections were imaged with LSM710 laser confocal scanning microscopy (Zeiss, Germany). The data were analyzed using ImageJ software.

In vitro T cell activation/restimulation and apoptosis assays

For activation and proliferation of TCR-Tg T cells, splenocytes from 2D2 mice or DO11.10 mice were stimulated in vitro in RPMI 1640 medium containing 10% fetal bovine serum, 2 mM glutamine, penicillin and streptomycin (100 U/ml), anti-CD3 (3 μg/ml; clone 145-2C11, BioLegend), and anti-CD28 (1 μg/ml; clone 37.51, BioLegend) or concanavalin A (1 μg/ml; Sigma-Aldrich). After 3 days, the activated T cells were washed and then cultured in complete RPMI 1640 medium containing recombinant human IL-2 (100 U/ml; R&D Systems). After 2 days, dead cells were removed by gradient centrifugation using Ficoll-Paque, and then the activated, live T cells were cultured with IL-2 (300 U/ml) overnight before apoptosis assays. For kill assays, triplicate wells in 96-well round-bottomed plates were seeded with 200 μl per well with 1×10^5/ml of activated 2D2 T cells and 6× irradiated splenocytes loaded with 10 to 160 μg/ml of the following antigens: MMPt, MP4, OVA proteins, or MOGp. Plate-bound anti-CD3ε (0.5, 5, 50, 500, and 5000 ng/ml) was used to restimulate activated T cells. Cell viability was determined by staining with propidium iodide (5 μg/ml) and flow cytometry collecting on a constant time of 20 s per sample. Percentage cell loss was calculated = {1 − [number of viable cells (restimulated)/number of viable cells (untreated)]} × 100.

Antigen-induced in vivo T cell apoptosis experiments

Day 5 activated T cells from 2D2 (MOGp-specific) or DO11.10 (OVAp-specific) mice were obtained as described above in the in vitro assay, and 6×10^6 of the IL-2 cultured T cells were adoptively transferred correspondingly into each of the *C57BL/6* or *BALB/c* mice that were pretreated with and without CsA (1.25 mg/kg) as indicated in fig. S8. These mice were then subjected to IV injections of the indicated antigen stimulations in the presence or absence of CsA as indicated in fig. S8 for 4 to 8 days. The splenocytes and lymph node cells were harvested and quantified for depletion by flow cytometry in constant time counting.

Enzyme-linked immunosorbent assay

Cell-free supernatants were harvested and assayed for mouse IL-10 (eBioscience) and IL-1β (eBioscience) according to the manufacturer′s instructions.

Immunoblot analysis

Immunoblotting was carried out as previously described (*78*). Primary antibodies were purchased from Cell Signaling Technology, Santa Cruz Biotechnology, or Beyotime (China). Secondary antibodies were from Beyotime.

Quantitative PCR analysis

RNA was extracted from mice SC tissue using the RNeasy Lipid Tissue Mini Kit (QIAGEN, USA) or from flow-sorted cells using the RNeasy Mini Kit (QIAGEN, USA) according to the manufacturer's instructions. The iScript cDNA Synthesis Kit (Bio-Rad) was used to prepare cDNA from 1 μg of RNA from each sample. Power SYBR Green PCR Master Mix (Applied Biosystems) was used for subsequent real-time reverse transcription PCR with specific primers for each gene on a 7900HT machine (ABI). We normalized expression to hypoxanthine phosphoribosyl transferase. Primer sequences are provided in table S1.

Proliferation assays

Splenocytes were prepared from wild-type, MMPt-, or vehicle-treated EAE mice at day 15 after one dose of MMPt treatment and then labeled with carboxyfluorescein diacetate succinimidyl ester (CFSE; 3 μM; eBioscience). Cells were then restimulated with MOGp (20 μg/ml) in vitro for 3 days. The frequency of T cells producing IL-17, IL-10, IFN-γ, FoxP3$^+$ T cells, and CFSE dilution was analyzed by flow cytometry.

Histological analysis

Mice were perfused with PBS, and spinal cords were collected and fixed in 10% formalin. Spinal cord sections were stained with hematoxylin and eosin for visualization of leukocyte infiltration and with toluidine blue or Luxol fast blue/periodic acid–Schiff stain for myelin sheath.

TUNEL staining

Apoptotic cells were assessed by TUNEL assay. Briefly, the spinal cord sections were deparaffinized in four changes of xylene and rehydrated through graded alcohol. The sections were stained using a standard procedure by a commercial vendor (Histolab). The tissue sections were visualized by basic fuchsin (red color) and then counterstained with hematoxylin (purple color).

Data analysis

Intravital cell movement was tracked and analyzed with Imaris 7.6 (Bitplane AG, Zurich, Switzerland, 641 RRID: SCR_007370) software. The mean velocity and arrest coefficient were calculated using Post-Track Object software (custom-designed software) as previously described (*79*). The arrest coefficient was calculated as the percentage of time that the instantaneous velocity of each cell was less than 2 μm/min. Cells with a mean velocity of less than 2 μm/min were defined as immotile (*80*).

Statistical analysis

Statistical analysis was performed using GraphPad Prism 5 (GraphPad Software Inc., La Jolla CA, USA, RRID: SCR_002798). For comparisons of two groups, the two-tailed unpaired *t* test was performed. The statistical analysis is described in each figure legend. Differences between or among groups are denoted as ns for nonsignificant, $^*P < 0.05$, $^{**}P < 0.01$, and $^{***}P < 0.001$.

Supplementary Materials

This PDF file includes:
Figs. S1 to S14
Legends for movies S1 to S3
References

Other Supplementary Material for this manuscript includes the following:
Movies S1 to S3

View/request a protocol for this paper from *Bio-protocol*.

REFERENCES AND NOTES

1. D. S. Reich, C. F. Lucchinetti, P. A. Calabresi, Multiple sclerosis. *N. Engl. J. Med.* **378**, 169–180 (2018).
2. Global, regional, and national burden of neurological disorders during 1990-2015: A systematic analysis for the Global Burden of Disease Study 2015. *Lancet Neurol.* **16**, 877–897 (2017).
3. H. E. Titus, Y. Chen, J. R. Podojil, A. P. Robinson, R. Balabanov, B. Popko, S. D. Miller, Preclinical and clinical implications of "Inside-Out" vs. "Outside-In" paradigms in multiple sclerosis etiopathogenesis. *Front. Cell. Neurosci.* **14**, 599717 (2020).
4. M. Naegele, R. Martin, The good and the bad of neuroinflammation in multiple sclerosis. *Handb. Clin. Neurol.* **122**, 59–87 (2014).
5. E. Bettelli, M. P. Das, E. D. Howard, H. L. Weiner, R. A. Sobel, V. K. Kuchroo, IL-10 is critical in the regulation of autoimmune encephalomyelitis as demonstrated by studies of IL-10- and IL-4-deficient and transgenic mice. *J. Immunol.* **161**, 3299–3306 (1998).
6. R. C. Coll, A. A. B. Robertson, J. J. Chae, S. C. Higgins, R. Muñoz-Planillo, M. C. Inserra, I. Vetter, L. S. Dungan, B. G. Monks, A. Stutz, D. E. Croker, M. S. Butler, M. Haneklaus, C. E. Sutton, G. Núñez, E. Latz, D. L. Kastner, K. H. G. Mills, S. L. Masters, K. Schroder, M. A. Cooper, L. A. J. O'Neill, A small-molecule inhibitor of the NLRP3 inflammasome for the treatment of inflammatory diseases. *Nat. Med.* **21**, 248–255 (2015).
7. J. M. Frischer, S. Bramow, A. Dal-Bianco, C. F. Lucchinetti, H. Rauschka, M. Schmidbauer, H. Laursen, P. S. Sorensen, H. Lassmann, The relation between inflammation and neurodegeneration in multiple sclerosis brains. *Brain* **132**, 1175–1189 (2009).
8. L. Steinman, Immunology of relapse and remission in multiple sclerosis. *Annu. Rev. Immunol.* **32**, 257–281 (2014).
9. A. Ben-Nun, H. Wekerle, I. R. Cohen, The rapid isolation of clonable antigen-specific T lymphocyte lines capable of mediating autoimmune encephalomyelitis. *Eur. J. Immunol.* **11**, 195–199 (1981).
10. R. Martin, H. F. McFarland, Immunological aspects of experimental allergic encephalomyelitis and multiple sclerosis. *Crit. Rev. Clin. Lab. Sci.* **32**, 121–182 (1995).
11. F. Mokhtarian, D. E. McFarlin, C. S. Raine, Adoptive transfer of myelin basic protein-sensitized T cells produces chronic relapsing demyelinating disease in mice. *Nature* **309**, 356–358 (1984).
12. D. Ontaneda, A. J. Thompson, R. J. Fox, J. A. Cohen, Progressive multiple sclerosis: Prospects for disease therapy, repair, and restoration of function. *Lancet* **389**, 1357–1366 (2017).
13. J. Sellner, P. S. Rommer, A review of the evidence for a natalizumab exit strategy for patients with multiple sclerosis. *Autoimmun. Rev.* **18**, 255–261 (2019).
14. C. H. Polman, P. W. O'Connor, E. Havrdova, M. Hutchinson, L. Kappos, D. H. Miller, J. T. Phillips, F. D. Lublin, G. Giovannoni, A. Wajgt, M. Toal, F. Lynn, M. A. Panzara, A. W. Sandrock; AFFIRM Investigators, A randomized, placebo-controlled trial of natalizumab for relapsing multiple sclerosis. *N. Engl. J. Med.* **354**, 899–910 (2006).
15. J. R. Berger, Classifying PML risk with disease modifying therapies. *Mult. Scler. Relat. Disord.* **12**, 59–63 (2017).
16. A. Compston, A. Coles, Multiple sclerosis. *Lancet* **372**, 1502–1517 (2008).
17. M. Gasim, C. N. Bernstein, L. A. Graff, S. B. Patten, R. El-Gabalawy, J. Sareen, J. M. Bolton, J. J. Marriott, J. D. Fisk, R. A. Marrie; CIHR team "Defining the burden and managing the effects of psychiatric comorbidity in chronic inflammatory disease", Adverse psychiatric effects of disease-modifying therapies in multiple sclerosis: A systematic review. *Mult. Scler. Relat. Disord.* **26**, 124–156 (2018).
18. A. J. Coles, D. A. S. Compston, K. W. Selmaj, S. L. Lake, S. Moran, D. H. Margolin, K. Norris, P. K. Tandon, Alemtuzumab vs. interferon β-1a in early multiple sclerosis. *N. Engl. J. Med.* **359**, 1786–1801 (2008).
19. G. Mancardi, R. Saccardi, Autologous haematopoietic stem-cell transplantation in multiple sclerosis. *Lancet Neurol.* **7**, 626–636 (2008).

20. L. Steinman, P. P. Ho, W. H. Robinson, P. J. Utz, P. Villoslada, Antigen-specific tolerance to self-antigens in protein replacement therapy, gene therapy and autoimmunity. *Curr. Opin. Immunol.* **61**, 46–53 (2019).
21. M. J. Lenardo, Interleukin-2 programs mouse αβ T lymphocytes for apoptosis. *Nature* **353**, 858–861 (1991).
22. L. Zheng, J. Li, M. Lenardo, Restimulation-induced cell death: New medical and research perspectives. *Immunol. Rev.* **277**, 44–60 (2017).
23. J. M. Critchfield, M. J. Lenardo, Antigen-induced programmed T cell death as a new approach to immune therapy. *Clin. Immunol. Immunopathol.* **75**, 13–19 (1995).
24. A. L. Snow, P. Pandiyan, L. Zheng, S. M. Krummey, M. J. Lenardo, The power and the promise of restimulation-induced cell death in human immune diseases. *Immunol. Rev.* **236**, 68–82 (2010).
25. G. Casella, J. Rasouli, A. Boehm, W. Zhang, D. Xiao, L. L. W. Ishikawa, R. Thome, X. Li, D. Hwang, P. Porazzi, S. Molugu, H. Y. Tang, G. X. Zhang, B. Ciric, A. Rostami, Oligodendrocyte-derived extracellular vesicles as antigen-specific therapy for autoimmune neuroinflammation in mice. *Sci. Transl. Med.* **12**, eaba0599 (2020).
26. G. D. Keeler, S. Kumar, B. Palaschak, E. L. Silverberg, D. M. Markusic, N. T. Jones, B. E. Hoffman, Gene therapy-induced antigen-specific tregs inhibit neuro-inflammation and reverse disease in a mouse model of multiple sclerosis. *Mol. Ther.* **26**, 173–183 (2018).
27. A. Lutterotti, H. Hayward-Koennecke, M. Sospedra, R. Martin, Antigen-specific immune tolerance in multiple sclerosis—Promising approaches and how to bring them to patients. *Front. Immunol.* **12**, 640935 (2021).
28. C. R. Gabaglia, A. T. Booker, T. A. Braciak, The potential for immunospecific therapy in multiple sclerosis based on identification of driver clones of the disease. *Crit. Rev. Immunol.* **40**, 237–246 (2020).
29. N. Kerlero de Rosbo, R. Milo, M. B. Lees, D. Burger, C. C. Bernard, A. Ben-Nun, Reactivity to myelin antigens in multiple sclerosis. Peripheral blood lymphocytes respond predominantly to myelin oligodendrocyte glycoprotein. *J. Clin. Invest.* **92**, 2602–2608 (1993).
30. M. Varrin-Doyer, A. Shetty, C. M. Spencer, U. Schulze-Topphoff, M. S. Weber, C. C. A. Bernard, T. Forsthuber, B. A. C. Cree, A. J. Slavin, S. S. Zamvil, MOG transmembrane and cytoplasmic domains contain highly stimulatory T-cell epitopes in MS. *Neurol. Neuroimmunol. Neuroinflamm.* **1**, e20 (2014).
31. J. M. Critchfield, M. K. Racke, J. C. Zúñiga-Pflücker, B. Cannella, C. S. Raine, J. Goverman, M. J. Lenardo, T cell deletion in high antigen dose therapy of autoimmune encephalomyelitis. *Science* **263**, 1139–1143 (1994).
32. C. E. Tadokoro, G. Shakhar, S. Shen, Y. Ding, A. C. Lino, A. Maraver, J. J. Lafaille, M. L. Dustin, Regulatory T cells inhibit stable contacts between $CD4^+$ T cells and dendritic cells in vivo. *J. Exp. Med.* **203**, 505–511 (2006).
33. X. Huang, H. Wu, Q. Lu, The mechanisms and applications of T cell vaccination for autoimmune diseases: A comprehensive review. *Clin Rev Allergy Immunol* **47**, 219–233 (2014).
34. J. Derdelinckx, P. Cras, Z. N. Berneman, N. Cools, Antigen-specific treatment modalities in MS: The past, the present, and the future. *Front. Immunol.* **12**, 624685 (2021).
35. F. Odoardi, N. Kawakami, Z. Li, C. Cordiglieri, K. Streyl, M. Nosov, W. E. F. Klinkert, J. W. Ellwart, J. Bauer, H. Lassmann, H. Wekerle, A. Flügel, Instant effect of soluble antigen on effector T cells in peripheral immune organs during immunotherapy of autoimmune encephalomyelitis. *Proc. Natl. Acad. Sci. U.S.A.* **104**, 920–925 (2007).
36. F. Odoardi, N. Kawakami, W. E. F. Klinkert, H. Wekerle, A. Flügel, Blood-borne soluble protein antigen intensifies T cell activation in autoimmune CNS lesions and exacerbates clinical disease. *Proc. Natl. Acad. Sci. U.S.A.* **104**, 18625–18630 (2007).
37. B. L. McRae, C. L. Vanderlugt, M. C. Dal Canto, S. D. Miller, Functional evidence for epitope spreading in the relapsing pathology of experimental autoimmune encephalomyelitis. *J. Exp. Med.* **182**, 75–85 (1995).
38. M. Yu, J. M. Johnson, V. K. Tuohy, A predictable sequential determinant spreading cascade invariably accompanies progression of experimental autoimmune encephalomyelitis: A basis for peptide-specific therapy after onset of clinical disease. *J. Exp. Med.* **183**, 1777–1788 (1996).
39. E. J. McMahon, S. L. Bailey, C. V. Castenada, H. Waldner, S. D. Miller, Epitope spreading initiates in the CNS in two mouse models of multiple sclerosis. *Nat. Med.* **11**, 335–339 (2005).
40. M. Lenardo, K. M. Chan, F. Hornung, H. McFarland, R. Siegel, J. Wang, L. Zheng, Mature T lymphocyte apoptosis–Immune regulation in a dynamic and unpredictable antigenic environment. *Annu. Rev. Immunol.* **17**, 221–253 (1999).
41. E. A. Elliott, H. I. McFarland, S. H. Nye, R. Cofiell, T. M. Wilson, J. A. Wilkins, S. P. Squinto, L. A. Matis, J. P. Mueller, Treatment of experimental encephalomyelitis with a novel chimeric fusion protein of myelin basic protein and proteolipid protein. *J. Clin. Invest.* **98**, 1602–1612 (1996).
42. S. D. Miller, D. M. Turley, J. R. Podojil, Antigen-specific tolerance strategies for the prevention and treatment of autoimmune disease. *Nat. Rev. Immunol.* **7**, 665–677 (2007).
43. D. P. McCarthy, M. H. Richards, S. D. Miller, Mouse models of multiple sclerosis: Experimental autoimmune encephalomyelitis and Theiler's virus-induced demyelinating disease. *Methods Mol. Biol.* **900**, 381–401 (2012).
44. L. Zheng, C. L. Trageser, D. M. Willerford, M. J. Lenardo, T cell growth cytokines cause the superinduction of molecules mediating antigen-induced T lymphocyte death. *J. Immunol.* **160**, 763–769 (1998).
45. M. Greter, F. L. Heppner, M. P. Lemos, B. M. Odermatt, N. Goebels, T. Laufer, R. J. Noelle, B. Becher, Dendritic cells permit immune invasion of the CNS in an animal model of multiple sclerosis. *Nat. Med.* **11**, 328–334 (2005).
46. M. Prinz, H. Schmidt, A. Mildner, K.-P. Knobeloch, U.-K. Hanisch, J. Raasch, D. Merkler, C. Detje, I. Gutcher, J. Mages, R. Lang, R. Martin, R. Gold, B. Becher, W. Brück, U. Kalinke, Distinct and nonredundant in vivo functions of IFNAR on myeloid cells limit autoimmunity in the central nervous system. *Immunity* **28**, 675–686 (2008).
47. C. Schläger, H. Körner, M. Krueger, S. Vidoli, M. Haberl, D. Mielke, E. Brylla, T. Issekutz, C. Cabañas, P. J. Nelson, T. Ziemssen, V. Rohde, I. Bechmann, D. Lodygin, F. Odoardi, A. Flügel, Effector T-cell trafficking between the leptomeninges and the cerebrospinal fluid. *Nature* **530**, 349–353 (2016).
48. J. Loos, S. Schmaul, T. M. Noll, M. Paterka, M. Schillner, J. T. Löffel, F. Zipp, S. Bittner, Functional characteristics of Th1, Th17, and ex-Th17 cells in EAE revealed by intravital two-photon microscopy. *J. Neuroinflammation* **17**, 357 (2020).
49. B. Rossi, G. Constantin, Live imaging of immune responses in experimental models of multiple sclerosis. *Front. Immunol.* **7**, 506 (2016).
50. G. Rougon, S. Brasselet, F. Debarbieux, Advances in intravital non-linear optical imaging of the central nervous system in rodents. *Brain Plast.* **2**, 31–48 (2016).
51. S. Stoll, J. Delon, T. M. Brotz, R. N. Germain, Dynamic imaging of T cell-dendritic cell interactions in lymph nodes. *Science* **296**, 1873–1876 (2002).
52. G. Mandolesi, A. Gentile, A. Musella, D. Fresegna, F. De Vito, S. Bullitta, H. Sepman, G. A. Marfia, D. Centonze, Synaptopathy connects inflammation and neurodegeneration in multiple sclerosis. *Nat. Rev. Neurol.* **11**, 711–724 (2015).
53. Y. Cao, B. A. Goods, K. Raddassi, G. T. Nepom, W. W. Kwok, J. C. Love, D. A. Hafler, Functional inflammatory profiles distinguish myelin-reactive T cells from patients with multiple sclerosis. *Sci. Transl. Med.* **7**, 287ra74 (2015).
54. M. S. Weber, T. Prod'homme, S. Youssef, S. E. Dunn, C. D. Rundle, L. Lee, J. C. Patarroyo, O. Stüve, R. A. Sobel, L. Steinman, S. S. Zamvil, Type II monocytes modulate T cell–mediated central nervous system autoimmune disease. *Nat. Med.* **13**, 935–943 (2007).
55. C. L. Mack, C. L. Vanderlugt-Castaneda, K. L. Neville, S. D. Miller, Microglia are activated to become competent antigen presenting and effector cells in the inflammatory environment of the Theiler's virus model of multiple sclerosis. *J. Neuroimmunol.* **144**, 68–79 (2003).
56. M. J. C. Jordão, R. Sankowski, S. M. Brendecke, Sagar, G. Locatelli, Y.-H. Tai, T. L. Tay, E. Schramm, S. Armbruster, N. Hagemeyer, O. Groß, D. Mai, Ö. Çiçek, T. Falk, M. Kerschensteiner, D. Grün, M. Prinz, Single-cell profiling identifies myeloid cell subsets with distinct fates during neuroinflammation. *Science* **363**, eaat7554 (2019).
57. I. Huitinga, N. van Rooijen, C. J. de Groot, B. M. Uitdehaag, C. D. Dijkstra, Suppression of experimental allergic encephalomyelitis in Lewis rats after elimination of macrophages. *J. Exp. Med.* **172**, 1025–1033 (1990).
58. M. M. Polfliet, P. H. Goede, E. M. van Kesteren-Hendrikx, N. van Rooijen, C. D. Dijkstra, T. K. van den Berg, A method for the selective depletion of perivascular and meningeal macrophages in the central nervous system. *J. Neuroimmunol.* **116**, 188–195 (2001).
59. M. M. Polfliet, F. van de Veerdonk, E. A. Döpp, E. M. van Kesteren-Hendrikx, N. van Rooijen, C. D. Dijkstra, T. K. van den Berg, The role of perivascular and meningeal macrophages in experimental allergic encephalomyelitis. *J. Neuroimmunol.* **122**, 1–8 (2002).
60. L. Ostendorf, P. Dittert, R. Biesen, A. Duchow, V. Stiglbauer, K. Ruprecht, J. Bellmann-Strobl, D. Seelow, W. Stenzel, R. A. Niesner, A. E. Hauser, F. Paul, H. Radbruch, SIGLEC1 (CD169): A marker of active neuroinflammation in the brain but not in the blood of multiple sclerosis patients. *Sci. Rep.* **11**, 10299 (2021).
61. A. Cugurra, T. Mamuladze, J. Rustenhoven, T. Dykstra, G. Beroshvili, Z. J. Greenberg, W. Baker, Z. Papadopoulos, A. Drieu, S. Blackburn, M. Kanamori, S. Brioschi, J. Herz, L. G. Schuettpelz, M. Colonna, I. Smirnov, J. Kipnis, Skull and vertebral bone marrow are myeloid cell reservoirs for the meninges and CNS parenchyma. *Science* **373**, eabf7844 (2021).
62. A. Wlodarczyk, M. Løbner, O. Cédile, T. Owens, Comparison of microglia and infiltrating $CD11c^+$ cells as antigen presenting cells for T cell proliferation and cytokine response. *J. Neuroinflammation* **11**, 57 (2014).
63. S. Gordon, J. Hamann, H. H. Lin, M. Stacey, F4/80 and the related adhesion-GPCRs. *Eur. J. Immunol.* **41**, 2472–2476 (2011).
64. D. Mrdjen, A. Pavlovic, F. J. Hartmann, B. Schreiner, S. G. Utz, B. P. Leung, I. Lelios, F. L. Heppner, J. Kipnis, D. Merkler, M. Greter, B. Becher, High-dimensional single-cell

mapping of central nervous system immune cells reveals distinct myeloid subsets in health, aging, and disease. *Immunity* **48**, 380–395.e6 (2018).
65. N. Villacampa, M. T. Heneka, Microglia: You'll never walk alone! *Immunity* **48**, 195–197 (2018).
66. I. Bechmann, J. Priller, A. Kovac, M. Böntert, T. Wehner, F. F. Klett, J. Bohsung, M. Stuschke, U. Dirnagl, R. Nitsch, Immune surveillance of mouse brain perivascular spaces by blood-borne macrophages. *Eur. J. Neurosci.* **14**, 1651–1658 (2001).
67. H. Li, G.-X. Zhang, Y. Chen, H. Xu, D. C. Fitzgerald, Z. Zhao, A. Rostami, CD11c $^{+}$ CD11b $^{+}$ dendritic cells play an important role in intravenous tolerance and the suppression of experimental autoimmune encephalomyelitis. *J. Immunol.* **181**, 2483–2493 (2008).
68. R. Yamasaki, H. Lu, O. Butovsky, N. Ohno, A. M. Rietsch, R. Cialic, P. M. Wu, C. E. Doykan, J. Lin, A. C. Cotleur, G. Kidd, M. M. Zorlu, N. Sun, W. Hu, L. Liu, J.-C. Lee, S. E. Taylor, L. Uehlein, D. Dixon, J. Gu, C. M. Floruta, M. Zhu, I. F. Charo, H. L. Weiner, R. M. Ransohoff, Differential roles of microglia and monocytes in the inflamed central nervous system. *J. Exp. Med.* **211**, 1533–1549 (2014).
69. M. Inoue, K. L. Williams, M. D. Gunn, M. L. Shinohara, NLRP3 inflammasome induces chemotactic immune cell migration to the CNS in experimental autoimmune encephalomyelitis. *Proc. Natl. Acad. Sci. U.S.A.* **109**, 10480–10485 (2012).
70. A. Lutterotti, S. Yousef, A. Sputtek, K. H. Stürner, J.-P. Stellmann, P. Breiden, S. Reinhardt, C. Schulze, M. Bester, C. Heesen, S. Schippling, S. D. Miller, M. Sospedra, R. Martin, Antigen-specific tolerance by autologous myelin peptide-coupled cells: A phase 1 trial in multiple sclerosis. *Sci. Transl. Med.* **5**, 188ra75 (2013).
71. H. I. McFarland, A. A. Lobito, M. M. Johnson, J. T. Nyswaner, J. A. Frank, G. R. Palardy, N. Tresser, C. P. Genain, J. P. Mueller, L. A. Matis, M. J. Lenardo, Determinant spreading associated with demyelination in a nonhuman primate model of multiple sclerosis. *J. Immunol.* **162**, 2384–2390 (1999).
72. C. L. Vanderlugt, S. D. Miller, Epitope spreading in immune-mediated diseases: Implications for immunotherapy. *Nat. Rev. Immunol.* **2**, 85–95 (2002).
73. J. Li, D. Qiu, Y. Liu, J. Xiong, Y. Wang, X. Yang, X. Fu, L. Zheng, G. Luo, M. Xing, Y. Wu, Cytomembrane infused polymer accelerating delivery of myelin antigen peptide to treat experimental autoimmune encephalomyelitis. *ACS Nano* **12**, 11579–11590 (2018).
74. Z. Hunter, D. P. McCarthy, W. T. Yap, C. T. Harp, D. R. Getts, L. D. Shea, S. D. Miller, A biodegradable nanoparticle platform for the induction of antigen-specific immune tolerance for treatment of autoimmune disease. *ACS Nano* **8**, 2148–2160 (2014).
75. G. Contarini, P. Giusti, S. D. Skaper, Active induction of experimental autoimmune encephalomyelitis in C57BL/6 Mice. *Methods Mol. Biol.* **1727**, 353–360 (2018).
76. M. J. Farrar, I. M. Bernstein, D. H. Schlafer, T. A. Cleland, J. R. Fetcho, C. B. Schaffer, Chronic in vivo imaging in the mouse spinal cord using an implanted chamber. *Nat. Methods* **9**, 297–302 (2012).
77. B. Schattling, K. Steinbach, E. Thies, M. Kruse, A. Menigoz, F. Ufer, V. Flockerzi, W. Brück, O. Pongs, R. Vennekens, M. Kneussel, M. Freichel, D. Merkler, M. A. Friese, TRPM4 cation channel mediates axonal and neuronal degeneration in experimental autoimmune encephalomyelitis and multiple sclerosis. *Nat. Med.* **18**, 1805–1811 (2012).
78. C. L. Lucas, H. S. Kuehn, F. Zhao, J. E. Niemela, E. K. Deenick, U. Palendira, D. T. Avery, L. Moens, J. L. Cannons, M. Biancalana, J. Stoddard, W. Ouyang, D. M. Frucht, V. K. Rao, T. P. Atkinson, A. Agharahimi, A. A. Hussey, L. R. Folio, K. N. Olivier, T. A. Fleisher, S. Pittaluga, S. M. Holland, J. I. Cohen, J. B. Oliveira, S. G. Tangye, P. L. Schwartzberg, M. J. Lenardo, G. Uzel, Dominant-activating germline mutations in the gene encoding the PI(3)K catalytic subunit p110δ result in T cell senescence and human immunodeficiency. *Nat. Immunol.* **15**, 88–97 (2014).
79. S. Hugues, A. Scholer, A. Boissonnas, A. Nussbaum, C. Combadière, S. Amigorena, L. Fetler, Dynamic imaging of chemokine-dependent CD8^{+} T cell help for CD8^{+} T cell responses. *Nat. Immunol.* **8**, 921–930 (2007).
80. A. Boissonnas, L. Fetler, I. S. Zeelenberg, S. Hugues, S. Amigorena, In vivo imaging of cytotoxic T cell infiltration and elimination of a solid tumor. *J. Exp. Med.* **204**, 345–356 (2007).
81. A. J. Wilk, A. Rustagi, N. Q. Zhao, J. Roque, G. J. Martinez-Colon, J. L. McKechnie, G. T. Ivison, T. Ranganath, R. Vergara, T. Hollis, L. J. Simpson, P. Grant, A. Subramanian, A. J. Rogers, C. A. Blish, A single-cell atlas of the peripheral immune response in patients with severe COVID-19. *Nat. Med.* **26**, 1070–1076 (2020).

Acknowledgments: We thank P. Jiang and B. Chao (National Institute of Allergy and Infectious Diseases) for technical assistance. We also thank S. Wohlstadter, R. Von Borstel, and other colleagues at Wellstat Immunotherapeutics for useful discussions and support. We thank J. Fritz, W. Comrie, J. Ravel, and B. Lo for critical discussions of the study. We thank S. Weber of LISB, NIAID and Bradley Otterson, NIH Library Writing Center, for manuscript editing assistance. **Funding:** This research work was supported by the Division of Intramural Research of the National Institute of Allergy and Infectious Diseases, NIH. We also thank Wellstat Immunotherapeutics and Pfizer Inc. J.L. was supported by the National Natural Science Foundation of China (32070912). Y.W. was supported by the National Key Research and Development Program of China (2016YFA0502204). Z.Z. was supported by the National Science Fund for Distinguished Young Scholars (81625012), Program for Huazhong University of Science and Technology (HUST) Academic Frontier Youth Team, and the Director Fund of Wuhan National Laboratory for Optoelectronics (WNLO). **Author contributions:** J.L., L.L., and K.B. designed and performed experiments, analyzed data, and prepared the manuscript. L.Z., W.L., and J.W.L. generated the MMPt protein. J.X. assisted with experiments. S.M.-M. carried out experiments and data analyses. Y.H.C. carried out human single-cell RNA sequencing analysis. L.Y. provided advice. L.Z. involved in design, carrying out experiments, data analyses, and manuscript preparation. Y.-z.W. and Z.Z. supervised experiments, and M.J.L. designed and supervised the research, analyzed data, and helped prepare the manuscript. **Competing interests:** M.J.L., J.W.L., L.Z., J.L., and W.L., all co-authors of this manuscript, are the co-inventors in the application patent no. 20210038685/WO/2016/145086, the only patent related to this work. The patent was filed by the U.S. National Institutes of Health. All authors declare that they have no other competing interests. **Data and materials availability:** All data needed to evaluate the conclusions in the paper are present in the paper and/or the Supplementary Materials.

Submitted 26 January 2022
Accepted 27 December 2022
Published 1 March 2023
10.1126/sciadv.abo2810